DIODE LASER ATOMIC SPECTROSCOPY

By

TYE ED BARBER

A DISSERTATION PRESENTED TO THE GRADUATE SCHOOL
OF THE UNIVERSITY OF FLORIDA IN PARTIAL FULFILLMENT
OF THE REQUIREMENTS FOR THE DEGREE OF
DOCTOR OF PHILOSOPHY

UNIVERSITY OF FLORIDA

1992

UNIVERSITY OF FLORIDA LIBRARIES

Copyright 1992

by

Tye Ed Barber

ACKNOWLEDGEMENTS

I thank my parents for their support and their guidance, and for always stressing the need for higher education. I also thank my brothers, Wade and Bart, for everything they have done for me.

I would like to acknowledge my research advisor, Dr. James D. Winefordner, for giving me freedom to pursue the work described in this dissertation. I have been fortunate enough to work with several postdocs: Piet Walters, Kin Ng, and Nico Omenetto. They have all greatly influenced me. I have also had the opportunity to work with several fellow students: Paul Johnson, Abdalla Ali, Mike Wensing, Steve Lehotay and Kimberly Ferrell.

I would especially like to thank Norma Ayala, who has helped me prepare many of my presentations, papers, and this dissertation. Without her constant encouragement and help, much of my work would not have been completed.

TABLE OF CONTENTS

page

ACKNOWLEDGMENTS iii

LIST OF TABLES vi

LIST OF FIGURES vii

ABSTRACT x

CHAPTERS

1. INTRODUCTION 1

2. DIODE LASERS 4

    Introduction 4
    Semiconductor Materials 4
    Diode Laser Characteristics 10
    Spectral Characteristics 11
    Laser Diode Aging and Failure 24

3. THEORY OF ATOMIC ABSORPTION AND ATOMIC FLUORESCENCE 26

    Introduction 26
    Spectral Line Profiles 29
    Methods of Measuring Atomic Absorption 33
    Atomic Fluorescence 37

4. DIODE LASER ATOMIC ABSORPTION 39

    Introduction 39
    Experimental 44
    Results and Discussion 56

5. DIODE LASER ATOMIC FLUORESCENCE 61

    Introduction 61
    Experimental 62

Results and Discussion 70

6. EVALUATION OF ABSOLUTE NUMBER DENSITIES BY DIODE LASER ATOMIC SPECTROSCOPY 73

Introduction 73
Theory 76
Case A 80
Case B 81
Case C 82
Experimental 86
Results and Discussion 93

7. CONCLUSIONS 105

APPENDIX QUALITATIVE COMPARISON OF THE SPECTRAL PROFILE OF A RUBIDIUM HOLLOW CATHODE LAMP AND RUBIDIUM ABSORPTION IN A FLAME 108

Experimental 109
Results and Discussion 115

REFERENCES 121

BIOGRAPHICAL SKETCH 125

LIST OF TABLES

page

2-1. Equipment Used to Measure the Emission Spectrum of a Diode Laser. 15

4-1. Detailed List of Equipment Used in AAS. 45

5-1. Detailed List of the Equipment Used. 63

6-1. Relationship of Photodiode Signal to the Integrated Intensity of the Laser Beam. 79

6-2. Partial List of Equipment Used for Absolute AAS (See Table 4-1 for Other Equipment). 91

A-1. Experimental Equipment for Measurement of Hyperfine Structure of Rb in a Hollow Cathode Lamp and a Flame. 110

LIST OF FIGURES

page

2-1. Energy Level Diagram of a Semiconductor Material. 6

2-2. A Diagram Showing the Elliptical Beam Emitted from a Diode Laser. 13

2-3. Spectrum of a Mitsubishi ML 4402 Semiconductor Laser. 17

2-4. Schematic Diagram of Experimental Set up Used to Measure the Emission Spectrum of a Diode Laser. 19

2-5. Spectrum of a Mitsubishi ML 4402 Semiconductor Laser. The Central Mode of the Laser Has Been Completely Absorbed by an Atomic Vapor Filter or Cell. 21

2-6. A Graphical Representation of a Tuning Curve of a Diode Laser. The Location of the Mode Hops Depends on the Direction of Tuning. 23

3-1. A Graphical Representation of an Absorption Profile. 28

3-2. A Plot of the Absorption Factor, α, Versus Frequency. 36

4-1. Block Diagram of the Experimental Set up. 47

4-2. Drawing Showing a Sinusoidal Modulation Ramp. The Ramp is Superimposed on Top of the Base Driving. In On/Off Modulation, the Laser is Modulated Onto Only Part of the Absorption Profile. In Across Modulation, the Laser is Modulated Across the Entire Absorption Profile. 49

4-3. Oscilloscope Traces Showing the Modulation Ramp (Upper Trace), the Absorption Signal (Middle Trace), and the Reference Waveform (Lower Trace). 52

4-4. Electronic Circuit Used to Shape the Absorption Signal of the Vapor Cell into the Reference Signal.. 55

4-5. Different Types of Modulated Signals. 58

5-1. Schematic Diagram of the Apparatus Used for Diode Laser Atomic Fluorescences. 66

5-2. Energy Level Diagram Showing the Rubidium Transitions Used in This Study. 69

6-1. Schematics and Terminology for the Three Proposed Experimental Arrangements. 78

6-2. Graphical Depiction of D_{Off} and D_{On}. 85

6-3. Detail Drawing of the Experimental Arrangement Used to Study Case A. 88

6-4. Detail Drawing of the Experimental Arrangement Used to Study Case C. 90

6-5. Water Jacket Used to Control Cell Temperature. 95

6-6. Rubidium Absorption in a Vapor Cell at 14.4 °C. 98

6-7. Plot of Absorption Factor Versus Rubidium Number Density. 100

6-8. Oscilloscope Trace Showing the Absorption of the Flame Superimposed on the Absorption of the Vapor Cell. 104

A-1. Experimental Arrangement Used to Measure Absorption in an Hollow Cathode Lamp. 112

A-2. Experimental Layout to Measure Atomic Fluorescence Simultaneously in the Hollow Cathode Lamp and Flame. 114

A-3. Rubidium Absorption Measured in a Hollow Cathode Lamp. 117

A-4. Rubidium Fluorescence Measured in a Hollow Cathode Lamp and in a Flame. 119

Abstract of Dissertation Presented to the Graduate School
of the University of Florida in Partial Fulfillment of the
Requirements for the Degree of Doctor of Philosophy

DIODE LASER ATOMIC SPECTROSCOPY

By

Tye Ed Barber

May 1992

Chairperson: James D. Winefordner
Major Department: Chemistry

A single mode semiconductor laser was used as the source for atomic absorption and atomic fluorescence spectroscopy. To overcome the problems of tuning the diode laser to the desired frequency and the frequency instabilities or drifts of the laser emission frequency, a new referencing approach was used. The emission frequency of the laser was modulated across the rubidium transition at 780.023 nm, and the absorption or fluorescence signal was detected in an air hydrogen flame. The atomic signals were measured by a lock-in amplifier. The reference signal for the lock-in amplifier was generated by the atomic absorption of rubidium in an atomic vapor cell. As the laser frequency fluctuated, no phase change occurred between the reference and analytical signals since they were both generated simultaneously by the same atomic transition. This eliminated any noise or signal loss that would have been caused by using a reference method which did not follow the fluctuations of the laser. The detection limits for rubidium atomic absorption and rubidium atomic fluorescence were 10 ng/ml and 0.2 ng/ml, respectively.

In addition, a simple method for evaluating absolute number densities in an atom reservoir was examined. It consists of measuring the difference in the integral absorption signals obtained from a reference cell and an analytical cell with a frequency-modulated diode laser as the source. The evaluation of the number density in the analytical cell is straightforward and does not even require knowledge of the absorption oscillator strength of the transition when the analytical cell is optically thin.

CHAPTER 1

INTRODUCTION

The purpose of the research presented in this dissertation is to develop and demonstrate new techniques using semiconductor diode lasers as the primary source for atomic spectroscopy. In atomic absorption and atomic fluorescence, the characteristics of the source in many cases determine the detection limit, sensitivity, and selectivity of the technique (1). During the past twenty five years, lasers have been demonstrated to offer many advantages over conventional sources such as hollow cathode lamps and xenon arcs. Lasers can have high spectral radiance and very narrow spectral line width. The tunability of dye laser systems has allowed a large number of elements to be analyzed by both atomic absorption and atomic fluorescence. Laser based atomic experiments have reported the best detection limits for some elements (2).

However, unlike molecular spectroscopy, lasers have only been employed in atomic spectroscopy for the analysis of a few actual samples on a routine basis. One of the reasons for this is that tunable dye laser systems are fairly expensive to purchase and maintain. A typical dye laser costs between $20,000 and $60,000 and, depending on what type of pump source is used, the yearly operating costs can range from $1,000 to $20,000 (3). In addition, laser systems can be difficult to operate and in some cases have a large percentage of down time. Operating dye lasers also generate large amounts of potentially hazardous waste which, due to environmental concerns, are difficult to dispose of safely. Thus, in most cases, the benefits of using lasers for analysis is outweighed by their disadvantages.

Due to the demands of the communications industry, diode lasers which are inexpensive, compact, and reliable have been developed. The operation and characteristics of diode lasers will be briefly described in Chapter 2. The average cost of a diode laser system is now only slightly greater than a hollow cathode lamp or electrodeless discharge lamp system. Therefore, the application of lasers to analytical atomic spectroscopy can again be considered as a viable alternative to other sources, especially for analysis at low concentration levels. Unfortunately, there are several problems associated with using diode lasers. Some of these problems will be addressed in Chapter 4. Also in this chapter, a new method to overcome the problem of frequency stability of the laser is presented and shown by atomic absorption. The application of a semiconductor laser to atomic fluorescence is described in Chapter 5.

The goal of many analytical chemist has been to develop a standardless or absolute method in which a single measurement could be used to determine the concentration of the analyte in a sample without the need for preparing a calibration curve to relate the measured signal to the concentration of the sample. A number of different techniques have been proposed to perform absolute measurement. The oldest method is the method of integral absorption.

The tunability of a diode laser has made possible a new way in which to measure the integral absorption. The theory and experimental details of using diode laser integral absorption for the evaluation of absolute number densities will be covered in Chapter 6.

CHAPTER 2

DIODE LASERS

Introduction

The first semiconductor laser or diode laser was constructed in 1964 (4). Early diode lasers were very inefficient and had to be cooled to liquid nitrogen temperature to operate. In 1970, scientists at AT&T Bell Laboratories were able to make a semiconductor laser which was able to produce a continuous-wave at room temperature, although it was not until almost a decade later, that diode lasers which were capable of thousands of hours of operation at room temperature became commercially available. Today, millions of diode lasers are produced each year. Most are highly efficient at converting electrical energy into light. Some manufacturers claim their lasers have lifetimes which exceed a quarter of a century of continuous operation (5). This chapter will briefly describe the characteristics of diode lasers. A more complete description can be found in references 6 thru 19.

Semiconductor Materials

In Figure 2-1, an energy level diagram for a semiconductor material is given. In this model, the solid is considered to have a large number of electronic levels

Figure 2-1. Energy Level Diagram of a Semiconductor Material.

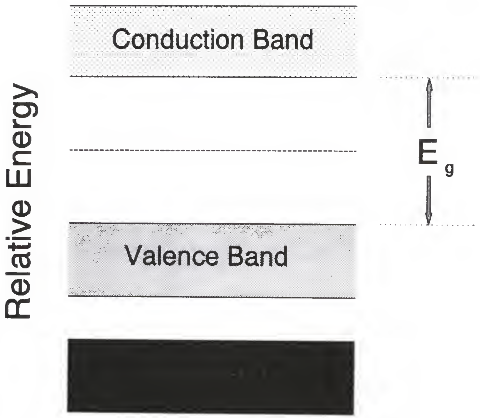
Relative Energy
Conduction Band
E g
Valence Band

with almost identical quantum numbers and similar energies. The electronic levels form pseudo-continuous energy bands. The occupation of the levels is governed by Fermi statistics and the Pauli exclusion principle. The inner electrons of the atoms are not involved in bonding and constitute the filled band. The valence band of the solid is occupied by the outer electrons of the atoms which form valence bonds. In order for the semiconductor to conduct electricity, electrons from the valence band must be excited to the conduction band. The energy difference between the valence band and the conduction band is the band gap energy, E_g (6).

The electronic properties of a semiconductor can be varied by the addition of foreign atoms to the semiconductor lattice. This process is referred to as doping. The doping material may have one more, n-type, or one less, p-type, valence electron than the major constituent of the semiconductor. In an n-type semiconductor, the current is carried by the movement of the extra electron. A p-type semiconductor conducts electricity by movement of electrons into the vacancy or hole left in the lattice by the doping material (7).

The band gap energy of semiconductor materials determines its optical properties. A photon with greater energy than or equal to the band gap energy will be absorbed promoting an electron from the valence band to the conduction band. A photon with less energy than the band gap will not be absorbed.

When p and n type semiconductors are brought together to form a p-n junction, electrons from the n side are attracted by the positive holes on the p side of the boundary and diffuse over to the p side (8). Similarly, holes on the p side are attracted to the n side. The electrons and holes combine forming a depletion region which is deficient in both electrons and holes. This region consists mainly of negative acceptor ions on the p side and positive donor ions on the n side. This creates a potential barrier which opposes the further diffusion of electrons and holes keeping the depletion region confined to a narrow layer at the junction.

By connecting a positive voltage to the p-type semiconductor and a negative to the n-type semiconductor, the junction is forward biased. The positive voltage repels holes and attracts electrons while the negative voltage repels electrons and attracts holes. If the voltage applied across the junction is greater than the potential barrier, current will flow through the semiconductor.

In the depletion region of a forward biased p-n junction, both electrons and holes are present simultaneously and can recombine either radiatively or nonradiatively. The energy of the emitted photons can be approximated by

$$h\nu \approx E_g$$

where h is Planck constant (J s), ν is the frequency of the photon (Hz), and E_g is the band gap energy (J) (9). The emitted photons can be absorbed forming electron-hole pairs. If the rate of emission exceeds the rate of absorption and the current flow is sufficiently high, population inversion can be achieved in which more electrons are in the excited state than in the ground state.

The first diode lasers were simple p-n junctions as described above. The resonant cavity of the lasers was formed by the cleaved facets of the semiconductor material. In a homojunction laser, p-type and n-type semiconductors are formed using the same bulk semiconductor material. The electrons and holes can flow across the junction to recombine on both sides. Since a homojunction laser has no mechanism to confine the charge carriers to the active region where lasing occurs, they are too inefficient for practical use and can not operate at room temperature.

Today, most diode lasers are made using double heterojunction technology. In a double heterojunction laser, a layer of p-type material is sandwiched between layers of p- and n-type material which have higher and lower band gap energies than the center of the p-type layer. This creates a potential well that confines the charge carriers to the central p layer which forms the active area. In addition, the active layer has a higher refractive index than the adjacent layers making this layer act as a waveguide. These factors make the double heterojunction laser highly efficient and operable at room temperature (10).

Normally, diode lasers are constructed so that they emit in stripes rather than across the entire width of the active layer. By using a striped geometry, the beam quality of the laser is greatly improved. The emitting stripes are, typically, a few micrometers wide. There are two basic types of striped lasers: gain guiding and index guiding. In gain guide lasers, the current flow is confined to a narrow stripe down the length of the chip. Even though there is no physical boundary to separate the stripe from the rest of the chip, only in the stripe region is current flow sufficient to produce population inversion and lasing. An index-guide laser is constructed so that there are refractive index changes which confine the emitted light to the striped region where lasing occurs (4).

Diode Laser Characteristics

The current vs. voltage curves of forward biased diode lasers resemble those of normal diodes. Little current flows through the diode until the applied voltage exceeds the junction potential and then it increases rapidly. In the operational region of a laser diode, small voltage changes cause large current changes; therefore, diode lasers are normally operated using constant current power supplies (11). Once the driving current of the laser exceeds the threshold current (the lowest current at which lasing occurs), the intensity emission from the laser will increase linearly with increasing current. Most low power diode lasers can be operated in the continuous or pulsed mode of operation. Because the diode responds rapidly to current modulation, the best diode lasers can be modulated in the gigahertz range.

The wavelength of light emitted from a laser diode is dependent on both the driving current and laser temperature. Current flowing through the diode laser perturbs the population in the valence and conduction bands and changes the refractive index of the semiconductor due to changes in electron-hole pair density. Increasing the current also causes thermal expansion of the laser cavity. The net effect is that the wavelength of the laser increases as current increases. The dependence of wavelength on current for a 780 nm laser is, typically, between 10 and 20 pm mA^{-1}. Changes in temperature result in changes in the band gap energy of the laser and in changes in the length of the laser cavity. Typical temperature dependence of a diode laser at 780 nm is 0.25 nm K^{-1} (12). Most diode lasers can be operated from -20 °C to 60 °C allowing the laser to be tuned over an approximately 20 nm range. The output power of a diode laser is also dependent on the temperature of the laser. Increasing the laser temperature will cause the threshold current to increase and will cause the power to decrease at a given current.

Due to the dimensions of the emitting aperture of a diode laser, the emitted beam is highly divergent and asymmetric, Figure 2-2. The active layer is, usually, compared to the emitted light, only a tenth of a wavelength thick and several wavelengths wide. Typical divergence parallel to the junction is 12 to 30°, and perpendicular to the junction is 24 to 60°. The output beam is also linearly polarized. The polarization ratio is, normally, greater than 100:1 (6).

Spectral Characteristics

For atomic spectroscopy, the most important characteristic of a laser diode is its spectral profile (13). Diode lasers which support single transverse modes (modes across the width of the laser), are often referred to as single mode. The output spectrum of the laser is determined by the longitudinal modes, which are the oscillation modes of a laser along the length of the cavity. The cleaved facets of the semiconductor form a Fabry-Perot cavity. The laser will oscillate at wavelengths that are integral multiples of twice the effective cavity length (14). The number of modes above the threshold, at a given current, depends on the gain spectrum which is the amount of amplification possible in a laser as a function of wavelength.

Figure 2-2. A Diagram Showing the Elliptical Beam Emitted from a Diode Laser.

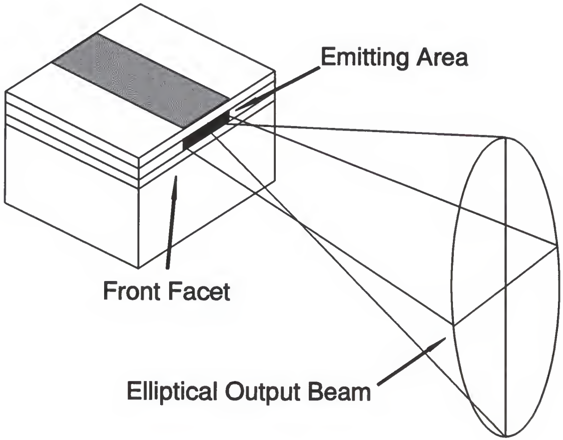
Emitting Area
Front Facet
Elliptical Output Beam

Index-guide lasers usually emit a central longitudinal mode which is more intense than the adjacent modes. Since the gain difference is very small between the central modes and the adjacent modes, lasing may still be observed from the side modes (15). Figure 2-3 shows the spectrum of a Mitsubishi ML4402 index-guide diode laser taken using the photodiode array experimental set up (see schematic diagram in Figure 2-4). The equipment used and the experimental conditions are given in Table 2-1. In order to be able to observe the side modes, the laser was tuned to the 780.023 nm transition of rubidium. After completely absorbing the central mode with an atomic vapor filter, see Chapter 6, the side modes could be observed by increasing the gain of the array, Figure 2-5. The intensity of the side modes can vary from manufacturer to manufacturer. Some index-guide lasers have side modes of up to 10% of the central mode. Because the side modes are not very effectively suppressed in some index-guide diode lasers, the laser may support multiple longitudal modes under modulation.

A graphical representation of the tuning curve of diode laser is given in Figure 2-6. The output of the laser increases linearly for approximately 300 pm and hop to a new wavelength region (16). The mode hop occurs when another longitudinal mode becomes preferred to the longitudinal mode supported by the laser cavity. The location, magnitude, and direction of the mode hop varies from laser to laser and depends upon the direction of tuning. Mode hopping creates holes in the tuning range of the laser preventing it from being tuned to some wavelengths (17).

Table 2-1. Equipment Used to Measure the Emission Spectra of a Diode Laser.

Monochromator	Spex 1870 0.5 m monochromator Dispersion 16A/mm Slit width 50 μm
Photodiode Array	Tracor Northern Model 5122A 1024 element intensified photodiode array
Data Acquisition Computer	Tracor Northern TN-6500
Diffuser	Melles Griot Opal Glass
Vapor Cell	Custom Made Pyrex 1" dia, 2" long 200 torr N_2
Heating Jacket	Custom made water jacket (see Chapter 6) Temperature 80°C

Figure 2-3. Spectrum of a Mitsubishi ML 4402 Semiconductor Laser.

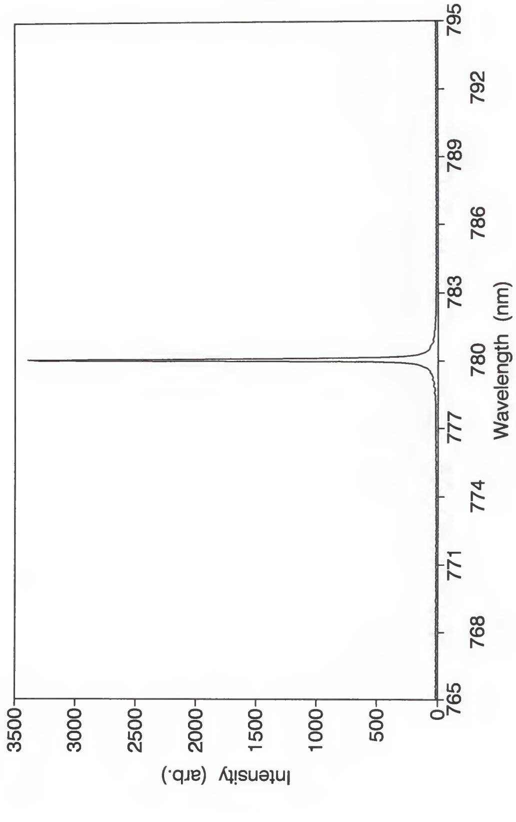
Intensity (arb.)
3500
3000
2500
2000
1500
1000
500
0
765
768
771
774
777
780
783
786
789
792
795
Wavelength (nm)

Figure 2-4.   Schematic Diagram of Experimental Set up Used to Measure the Emission Spectrum of a Diode Laser.

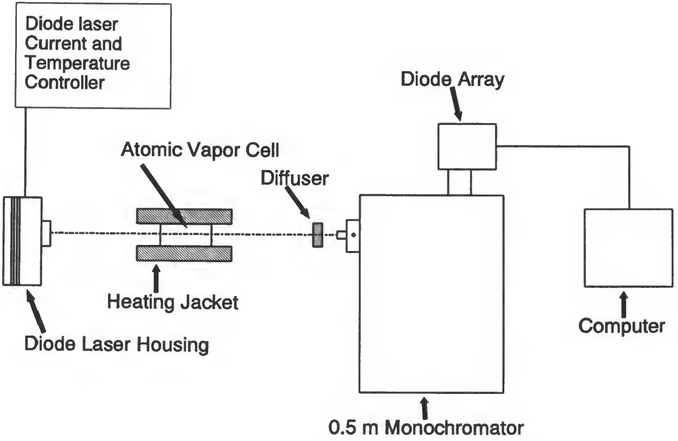
Diode laser
Current and
Temperature
Controller
Atomic Vapor Cell
Diffuser
Diode Array
Heating Jacket
Computer
Diode Laser Housing
0.5 m Monochromator

Figure 2-5. Spectrum of a Mitsubishi ML 4402 Semiconductor Laser. The Central Mode of the Laser has been Completely Absorbed by an Atomic Vapor Filter or Cell.

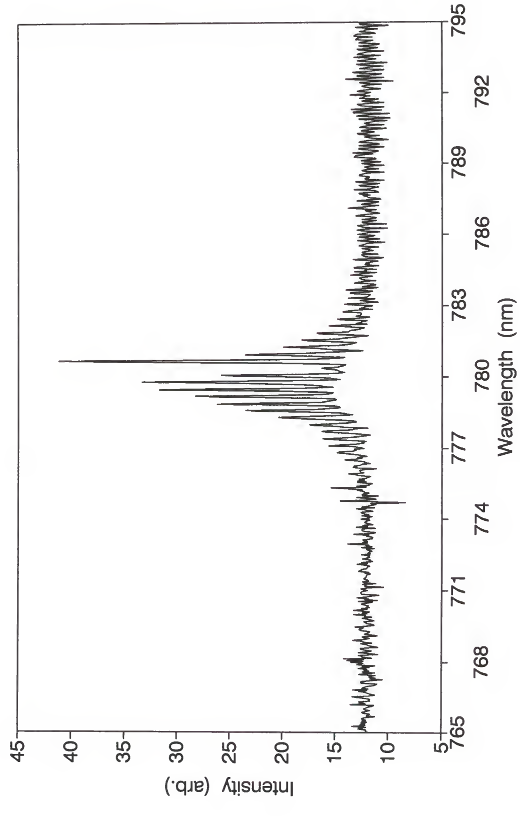
Intensity (arb.)
45
40
35
30
25
20
15
10
5
765
768
771
774
777
780
783
786
789
792
795
Wavelength (nm)

Figure 2-6. A Graphical Representation of a Tuning Curve of a Diode Laser. The Location of the Mode Hops Depends on the Direction of Tuning.

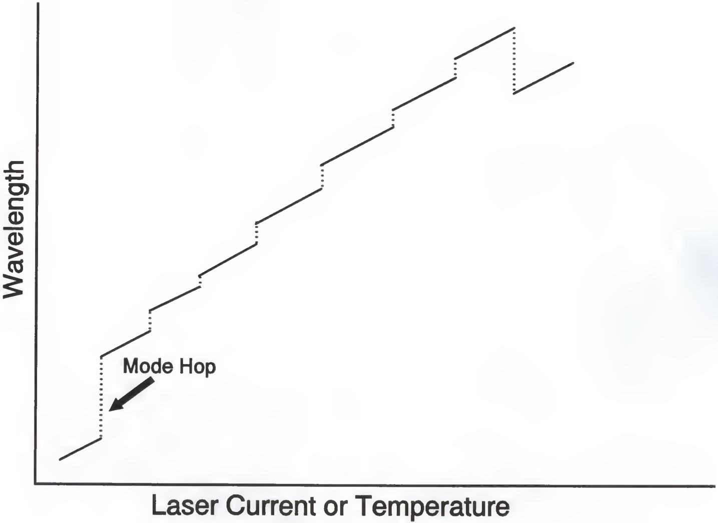
Wavelength
Mode Hop
Laser Current or Temperature

Diode lasers are also very sensitive to reflections of emitted light back onto the emitting area, Figure 2-2. Optical feedback can drastically change the emission spectrum of the laser, because it can allow different longitudinal modes to be supported by the laser cavity. Feedback can result in spectral line broadening, shifts in lasing frequency, and mode hopping (15,18).

Laser Diode Aging and Failure

The tuning characteristics of a semiconductor laser change with operation. During the first 100 hours of operation, the tuning properties of the laser drastically change (5,13,16,17). This is the result of diffusion of the doping material and impurities in the semiconductor lattice and of defect formation in the semiconductor crystal. Some manufacturers operate their lasers for a period of time before marketing to minimize the aging observed by the user. As a result of aging, a diode laser may not be able to be tuned to the same wavelength after a period of usage. Aging greatly reduces the effective life of a diode laser for atomic spectroscopy. The lifetime, defined as the ability to be tuned to 780.023 nm, of a ML 4402 diode laser has been observed to range from 20 to over 600 hours of operation.

Diode lasers can be destroyed in a number of ways (16). Semiconductor lasers are very sensitive to static electricity. To prevent damage, the manufacturers recommendations for handling and installation of the laser must be followed (19). For example, voltage spikes from improperly designed power supplies can destroy the laser. Also, diode lasers can be destroyed by operation at very high current levels. At very high currents, the photon flux at the emitting aperture of the laser diode becomes too high and the facet of the laser will be destroyed. Most diode lasers can be operated at powers up to five times the rated maximum power, but some laser manufacturers rate their lasers at 75% of the maximum power at which catastrophic failure occurs, once the facet of the laser is damaged, laser failure will occur. Although lasers can be operated at higher than rated powers and can be operated at higher than rated temperatures, such operation increases processes which will shorten the laser's lifetime (13).

CHAPTER 3

THEORY OF ATOMIC ABSORPTION AND ATOMIC FLUORESCENCE

Introduction

The theory of atomic absorption and atomic fluorescence has been extensively reviewed in the literature (1,20-26). Its inclusion here is to clarify some of the derivations in later chapters. The processes of atomic absorption and emission involve the transition of electrons between specific energy states due to interaction with electromagnetic radiation. In atomic absorption, an electron is excited to a higher energy by the atom absorbing the energy of a photon. If the excited electron relaxes to a lower energy level by the emission of a photon, the process is called atomic fluorescence.

The absorption of radiation by a homogeneous layer of atoms of thickness ℓ (cm) can be described by the well known Beer-Lambert law,

$$I_t(\nu) = I_o(\nu)\, e^{-k(\nu)\ell} \qquad \text{3-1}$$

where $I_t(\nu)$ and $I_o(\nu)$, respectively, are the intensity of the incident beam and transmitted beam through the sample, and $k(\nu)$ is the absorption coefficient (cm^{-1}). Intensity refers to any measure of radiation which can be related to the radiation flux. Figure 3-1 shows a graphical representation of an absorption profile. The absorption coefficient can be related to concentration by using the thermodynamic

Figure 3-1. A Graphical Representation of an Absorption Profile.
$I_o(\nu)$ - Incident Intensity
$I_a(\nu)$ - Intensity Absorbed
$I_t(\nu)$ - Intensity Transmitted

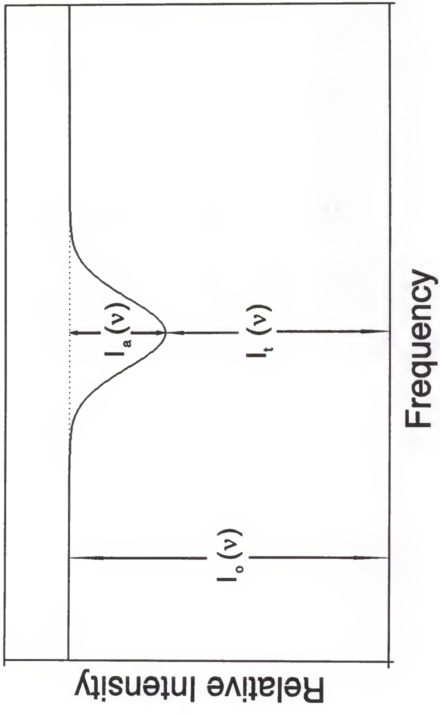
Relative Intensity
Frequency
I_o(ν)
I_a(ν)
I_t(ν)

equilibrium between radiation and the atoms shown by Einstein or by classical dispersion theory. The integral absorption coefficient is given by

$$\int_0^{\infty} k(\nu)d\nu = \frac{\pi e^2}{mc} n_a f \qquad 3\text{-}2$$

where e is the electron charge (C), c is the velocity of light (cm s^{-1}), m is the electron mass (g), n_a is the number density of atoms which are capable of absorbing radiation (cm^{-3}), and f is the absorption oscillator strength (dimensionless), which is a correction factor applied to classical theory and can be described as the average number of electrons per atom which are capable of being excited by the incident radiation.

Spectral Line Profiles

Even though the integral absorption coefficient does not depend upon factors except number density and several constants, the magnitude of the absorption coefficient at a discrete wavelength depends upon the spectral width of the atomic absorption profile. The profile of an atomic transition is determined by the broadening mechanisms and by the hyperfine structure of the transition. The major contributions to line broadening are lifetime broadening and Doppler broadening.

Because the levels in an atomic system can undergo various radiative and collisional processes, the excited states have finite lifetimes. This results in uncertainties in the energies of both states. According to the Heisenberg uncertainty principle, uncertainties in the energy of a state will give rise to a frequency distribution of the photons which are emitted or absorbed. The resulting broadening is called natural broadening which is a result of the radiative lifetime of the transition. The natural line width is normally insignificant in an analytical system when compared to other types of line broadening.

A more important type of line broadening is collisional broadening. Collisions between atoms or molecules perturb the lower and excited levels of the atom leaving the atom in either the same energy level, adiabatic collision, or in a different energy level, diabatic collision. Diabatic collisional broadening is often negligible compared to adiabatic collisional broadening.

Adiabatic collisions with a foreign gas not only cause broadening of the spectral line, but also shifting of the line center and asymmetry between the wings of the profile and the line center. This type of collisional broadening is often referred to as Lorentz broadening or foreign gas broadening. From classical theory, the foreign gas collisional broadening half width, $\Delta\nu_a$ (s^{-1}), can be described by the equation

$$\Delta\nu_a = \left(\frac{2kT}{\pi\mu}\right)^{\frac{1}{2}}\left(\frac{2}{\pi}\right)\sigma n_x \tag{3-3}$$

where k is the Boltzmann constant ($g\ cm^2\ s^{-2}\ K^{-1}$), T is the temperature (K), μ is the reduced mass (g), σ is the optical cross section for adiabatic collision broadening (cm^2), and n_x is the density of the perturbers (cm^{-3}).

If the natural and collisional broadening are assumed to be mutually independent, the sum of their half-width is the total Lorentzian profile,

$$\Delta\nu_L = \Delta\nu_N + \Delta\nu_C \qquad 3\text{-}4$$

where $\Delta\nu_L$, $\Delta\nu_N$, and $\Delta\nu_C$ are the Lorentzian profile, natural, and collisional half-widths, respectively. Since the adiabatic and diabatic collisions are not mutually independent, the collisional half-width is not simply the sum of the different types of collisional broadening. It is often found that $\Delta\nu_a >> \Delta\nu_N$ and that $\Delta\nu_a$ is much greater than the diabatic collisional width, so that $\Delta\nu_L = \Delta\nu_N \approx \Delta\nu_c$.

The thermal motion of the absorbing atoms along the observation path in an atom reservoir cause a distribution of velocities among the detected atoms. Making them appear at different frequencies depending upon the direction of the motion relative to the point of observation. This type of broadening is termed Doppler broadening; the Doppler half width, $\Delta\nu_D$, (s^{-1}), is given by

$$\Delta\nu_D = 2\left(\frac{2\sqrt{\ell n2kT}}{m_a}\right)^{\frac{1}{2}}\frac{\nu_m}{c} \qquad 3\text{-}5$$

where ν_m is the central frequency of the spectral line profile, and m_a is the mass of the absorbing atom.

Because Doppler broadening produces a Gaussian profile and collisional broadening produces a Lorentzian profile, the overall spectral line shape is a convolution of Gaussian and Lorentzian functions. If line asymmetry is ignored and the two types of broadening are assumed to be independent, the convoluted profile can be calculated by the Voigt equation. The Voigt integral $\delta(a,y)$ is given by

$$\delta(a,y) = \frac{a}{\pi}\int_{-\infty}^{\infty}\frac{e^{-y^2}}{(a-y)^2+a^2}dy \qquad 3\text{-}6$$

where

$$y=2\frac{(\nu-\nu_m)}{\Delta\nu_D}\sqrt{\ln 2} \qquad 3\text{-}7$$

and

$$a = \frac{\Delta\nu_L}{\Delta\nu_D}\sqrt{\ln 2} \qquad 3\text{-}8$$

The a term is called the damping constant (dimensionless). The Voigt integral can not be solved analytically, but a number of methods have been developed to approximate the solution (27,28).

An important, but often ignored, contribution to the effective profile of a spectral line observed in an experiment is the hyperfine structure of the transition (see Appendix). Hyperfine structure can result from isotope effects or from the interaction of a nonzero nuclear spin with the electrons. The hyperfine structure can only be neglected when the hyperfine splitting is much less than the Doppler and Lorentzian broadening. If the hyperfine splitting is much greater than the other contribution to line broadening, each hyperfine component must be treated as a separate line. The most complex case is when hyperfine splitting is approximately the same magnitude as the Doppler and Lorentzian broadening. In this case, it is necessary to calculate the profile for each hyperfine component, and to sum the profiles to determine the line shape (23).

Methods of Measuring Atomic Absorption

The strength of the absorption is expressed by the absorption factor α,

$$\alpha = \frac{I_a(\nu)}{I_o(\nu)} \qquad 3\text{-}9$$

where $I_a(\nu)$ and $I_o(\nu)$ are the intensity absorbed and the incident intensity, respectively. The ratio of the transmitted intensity $I_t(\nu)$ to the incident intensity $I_a(\nu)$ defines the transmission factor $T(\nu)$,

$$I_t(\nu) = I_o(\nu) - I_a(\nu) \qquad 3\text{-}10$$

$$T(\nu) = \frac{I_t(\nu)}{I_o(\nu)} \qquad 3\text{-}11$$

The absorbance, A, is defined as

$$A(\nu) = -\log_{10} T(\nu) \qquad 3\text{-}12$$

From the Beer-Lambert law, it is found that

$$A(\nu) = 0.4343\ k(\nu)\ell \qquad 3\text{-}13$$

which shows that absorbance is directly proportional to the absorption coefficient. $k(\nu)$ can be written as

$$k(\nu) = \sigma(\nu)\ n_A \qquad 3\text{-}14$$

where $\sigma(\nu)$ is the atomic absorption cross section and n_A is the atomic density (cm^{-3}) of the absorbing atoms.

Figure 3-2 shows a representation of a plot of α versus frequency. Instrumentally, the absorption factor is measured over a fixed spectral region of $\Delta\nu_s$ centered at the frequency of maximum absorption, ν_m. $\Delta\nu_s$ could be the bandpass of a monochromator or the spectral width of a line emitted from a hollow cathode lamp. $I_o(\nu)$ is the measured signal for the blank with a certain $\Delta\nu_s$. $I_t(\nu)$ is the measured signal for the sample with the same $\Delta\nu_S$. Equation 3-9 can be written as

$$\alpha = \frac{I_o(\nu) - I_t(\nu)}{I_o(\nu)} \qquad 3\text{-}15$$

$$\alpha = \frac{\int_{\Delta\nu_s} I_o(\nu)d\nu - \int_{\Delta\nu_s} I_o(\nu)e^{-k(\nu)\ell}d\nu}{\int_{\Delta\nu_s} I_o(\nu)d\nu} \qquad 3\text{-}16$$

If $\Delta\nu_S$ is narrow enough $k(\nu)$ can be considered as a constant over $\Delta\nu_S$ and equal to its maximum value, k_m at ν_m. The peak absorption factor is then

$$\alpha_m = 1-\exp[-\sigma_m n_A \ell] \qquad 3\text{-}17$$

It can be shown that

$$\sigma_m = \left(\frac{\pi e^2}{mc}\right)\frac{f}{\Delta\nu_{eff}} \qquad 3\text{-}18$$

where $\Delta\nu_{eff}$ is the effective half-width of the absorption determined by the overall line profile. Substituting Eq. 3-18 into Eq. 3-17, α_m is given by

$$\alpha_m = \left(\frac{\pi e^2}{mc}\right)\frac{f}{\Delta\nu_{eff}}n_A\ell \qquad 3\text{-}19$$

Figure 3-2. A Plot of the Absorption Factor, α, Versus Frequency.

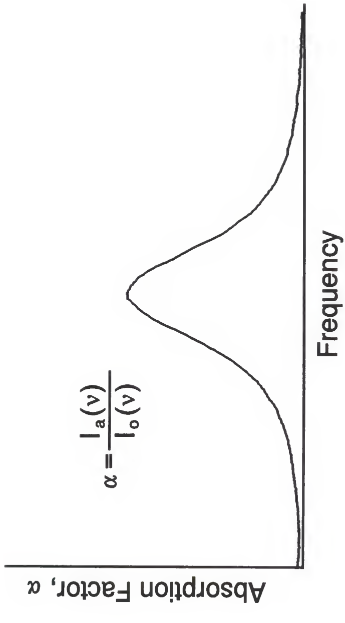
Absorption Factor, α
α = $\frac{I_a(\nu)}{I_o(\nu)}$
Frequency

showing that the peak absorption factor is dependent on the absorption profile of the transition.

When the atomic absorption is measured over the entire line profile using a continuum source and a monochromator, the absorption factor, α_c, at low optical thickness, $k_\nu \ell << 1$, is

$$\alpha_c = \frac{1}{\Delta \nu_s}\left(\frac{\pi e^2}{mc}\right) f n_A \ell \qquad \text{3-20}$$

The above equation shows that α_c is independent of spectral line profile at low optical densities, but is dependent on the bandpass $\Delta \nu_s$ of the monochromator. At high optical densities, $k_\nu \ell >> 1$, α_c is given by

$$\alpha_c = \frac{1}{\Delta \nu_s}\sqrt{\left(\frac{\pi e^2}{mc}\right) f n_A \ell \Delta \nu_{eff}} \qquad \text{3-21}$$

Atomic Fluorescence

Atomic fluorescence occurs when an electron is excited to a higher level by the absorption of a photon and a photon of light is emitted when it relaxes. If the fluorescence is at the same wavelength as the excitation source, it is referred to as resonance fluorescence. When fluorescence occurs at a different wavelength then absorption, it is called nonresonance fluorescence. At low optical densities, the intensity of the atomic fluorescence, Φ_F, with a narrow excitation source (spectral width of the source is much less than the absorption spectral width) is

$$\Phi_F = \left(\frac{\pi e^2}{mc}\right)\frac{fY\ell n_A\Phi_o}{\Delta\nu_{eff}} \qquad 3\text{-}22$$

where Y is the fraction of the absorbed radiant power emitted as fluorescence radiant power, and Φ_o is the intensity of the source.

CHAPTER 4

DIODE LASER ATOMIC ABSORPTION

Introduction

Semiconductor lasers were first used in atomic spectroscopy in 1968 just four years after the first diode laser was constructed (13). Because of the limitations of early diode lasers, they were only employed in a few experiments. Dye lasers, which were invented after the diode laser, were used almost exclusively for atomic spectrometry experiments requiring tunability, monochromaticity, coherence, and/or the intensity of a laser source. Semiconductor lasers are now very efficient, inexpensive, and can operate continuously at room temperature. Diode lasers have been shown to be excellent sources for analytical molecular spectroscopy (29), but there are several difficulties associated with using diode lasers as a primary source for atomic spectroscopy (16,17). Currently, the lowest wavelength obtainable by commercial semiconductor lasers is 620 nm. This limits the number of elements which can be analyzed using ground state transitions to the alkali metals and a few other elements. Since the emission spectra of the laser can change with optical feedback, it is necessary to design the optics to avoid reflections back into the laser (15). More serious problems are tuning the laser to the desired wavelength and maintaining the laser at that wavelength.

For atomic spectroscopy, it is necessary to tune the laser to the specific wavelength at which the atomic transitions occur. Most of the frustrations by researchers using diode lasers without external optics has been tuning the laser. Since diode lasers mode hop and the location of the mode hops are unknown, it may not be possible to tune an individual diode laser to the required wavelength (17). Therefore, unless special arrangements are made with the supplier, it is necessary to purchase several diode lasers before trying an experiment in order to ensure that at least one diode laser is tunable to the required wavelength. This adds additional cost to semiconductor laser experiments, but since the prices for most low power lasers range from $15 to $100 this is normally not a major expense. The nominal wavelength specified at certain operating conditions by the manufacturer may be several nanometers different than the wavelength observed experimentally. In addition, the current/wavelength and temperature/wavelength relationships vary from laser to laser. Because of these factors, it is almost futile to try to tune the laser to the desired wavelength based upon manufacturer specifications and wavelength relationships.

In order to tune the laser, most researchers use some type of optical spectrum analyzer to measure the emission wavelength of the laser. By continuously monitoring the laser, it is possible to vary the current/temperature combinations to obtain the desired wavelength. By using an atomic fluorescence or atomic absorption signal, the laser is then tuned to the resonance wavelength (16).

Diode lasers can have very poor frequency stability due to their sensitivity to small current and temperature variations. Several methods have been developed to stabilize the frequency of diode lasers (30-32), including procedures which often involve locking the laser to an external optical reference. The optical reference is normally a Fabry-Perot interferometer, an optogalvanic cell, or a vapor cell. By applying a small modulation to the laser's emission frequency, it is possible to use lock-in electronics to control the laser's temperature or current to maintain the desired wavelength. Optical feedback, which normally degrades the lasers performance, can also be used to stabilize the laser.

Because of their narrow spectral line width, < 20 MHz, and tunability, diode laser have been used extensively in atomic physics (13,16,17,33). Most of these studies involve high resolution spectroscopy of the alkali metals. Some of the physical properties which have been studied are hyperfine structure, absorption cross sections, collisional cross section, and photon echoes.

Because of the limited wavelengths available from semiconductor lasers and the difficulty of tuning them, diode lasers have not been widely used for analytical atomic spectroscopy. Some researchers have used diode lasers as one of the excitation steps in multiple step excitation schemes (34). This has extended the number of elements which can be measured, but involves other laser systems negating the benefits of the diode laser.

Since atomic absorption is the most common type of atomic spectroscopy, there has been much interest in replacing hollow cathode lamps with diode lasers.

Several researchers have employed semiconductor lasers as the primary for atomic absorption spectroscopy (AAS) (35-38). Ng *et al.* have shown that a multimode diode laser could be used as the source for lithium AAS. By utilizing a 1 m monochromator and a photodiode array, it was possible to resolve the modes emitted by the laser. One of the modes was tuned to the 670 nm transition of lithium and adjacent modes were used for background correction. The results were very similar to those obtainable with AAS using a hollow cathode lamp.

Ideally, a single mode diode laser could be used as a direct replacement for a hollow cathode lamp. In this type of arrangement, the only required components would be the diode laser and controllers, an atomizer, and a detector. Since a single mode diode laser emits a single wavelength and because its power is normally a few milliwatts, a photodiode without a monochromator can be used as the detector (39,40). Hergenröder and Niemax employed multiple diode lasers for the simultaneous determination of Rb and Ba in a graphite furnace. By modulating the lasers at different frequencies, they were able to use a single photodiode as a detector. Their results were over an order of magnitude worse than a electrodeless discharge lamp graphite furnace AA.

In most of the papers published on diode laser atomic absorption spectroscopy, the authors utilized only current and temperature stabilization, without any reference to the emitted wavelength to maintain the required wavelength. This approach required that the temperature and current be highly regulated for sufficient wavelength stability in order to obtain low detection limits. Much better results could have been achieved in some cases by frequency locking the laser. However, this would have added some complexity to simple absorption type experiments and the expense, at the current time, would not make it feasible for routine analyses.

In this work, a different approach was taken. Instead of trying to tune the laser to the wavelength of the atomic transition, the wavelength of the laser was modulated by modulating the driving current of the laser. The atomic absorption was measured as the wavelength of the laser scanned across the atomic transition. Since the temperature and base driving current of the laser could drift, resulting in a change in the base wavelength of the laser, the location of the absorption with respect to the current ramp could change. This could cause a phase change between the beginning of the modulation ramp and the absorption signal. To prevent this from affecting the absorption signal measured by a lock-in amplifier, the reference signal for the lock-in was generated by rubidium absorption in a separate atom reservoir than the analytical reservoir. Since the reference signal and the analytical signal were both due to the 780.023 nm transition of rubidium, there could be no phase change between them. By using this reference, frequency fluctuations with respect to the modulation ramp were not detected as noise by the lock-in amplifier. Because it was not necessary to tune directly to the wavelength of the atomic transition or to maintain the laser at the desired wavelength, this approach greatly simplified using a diode laser as a source for AAS (41).

Experimental

Figure 4-1 shows a block diagram of the experimental set up. The equipment is listed in Table 4-1. The diode laser was mounted in a commercial housing and was maintained at -4.5°C by a thermoelectric cooler. The housing was constantly flushed with nitrogen to avoid condensation on the laser or the optics. To aid the cooling process, a small fan was pointed at the housing's heat sink. The driving current of the laser was modulated by superimposing a sinusoidal or triangular waveform on top of the base current of the laser, Figure 4-2. The laser beam was collimated, and passed through the center of an air-hydrogen flame. Part of the beam was diverted by a beam splitter through an atomic vapor cell. Since the intensity of the laser emission varied with modulation of the current, it was necessary to monitor the intensity before and after each atom reservoir. This was accomplished by a pair of beam splitters and photodiodes in each case, as shown in Figure 4-1. The photodiode before the atom reservoirs served as a reference to the laser's intensity.

The output from each of the photodiodes, operating in the photovoltaic mode, was terminated in a 10 kΩ ten turn potentiometer. It was necessary to adjust the beam splitters and scan the laser beams over the surfaces of the photodiodes in order to obtain similar responses from each photodiode in a particular set. The voltages across the potentiometers were compared by an AD524 instrumentation amplifier. When the beam splitters and potentiometers were properly adjusted, the modulation ramp measured by each photodiode cancelled giving a constant voltage

Table 4-1. Detailed List of Equipment Used in AAS.

Diode laser	Model No. ML4102, Mitsubishi Electric Corp., Tokyo, Japan
Laser diode housing	Model No. LDM-4412, ILX Lightwave Corp., Bozeman, MT
Current source	Model LDX-3620, ILX Lightwave Corp., Bozeman, MT
Temperature controller	Model No. LDT-5910, Temperature controller, ILX Lightwave Corp., Bozeman, MT
Function generator	Model No. 110, Function generator, Wavetek, San Diego, CA
Burner	Conventional premixed AA burner, Perkin-Elmer, Norwalk, CT
Lock-in amplifier	Model No. 391A, Frequency range 0.1-10 kHz, Ithaco Dynatrac, Ithaca, NY
Computer interface	Model No. SR245, Stanford Research, Palo Alto, CA
Photodiodes	Flame; Model No. UDT 10DP/SB, Vapor Cell Model No. UDT Pin VV 100, United Detector Technologies, Hawthorne, CA
Oscilloscope	Model No. 5403A, 500 MHz, Hewlett Packard, Rockville, MD
Photodiode array	Model #5122A, TN-6500, Tracor Northern, Middleton, WI
Spectrometer	Model No. 1870, Spex Industries, Inc., Metuchen, NJ

Figure 4-1. Block Diagram of the Experimental Set up Used for Diode Laser AA. The Laser Housing Contains the Diode Laser, Collimating Lens, Thermoelectric Cooler, and Heat Sink (Not Shown).

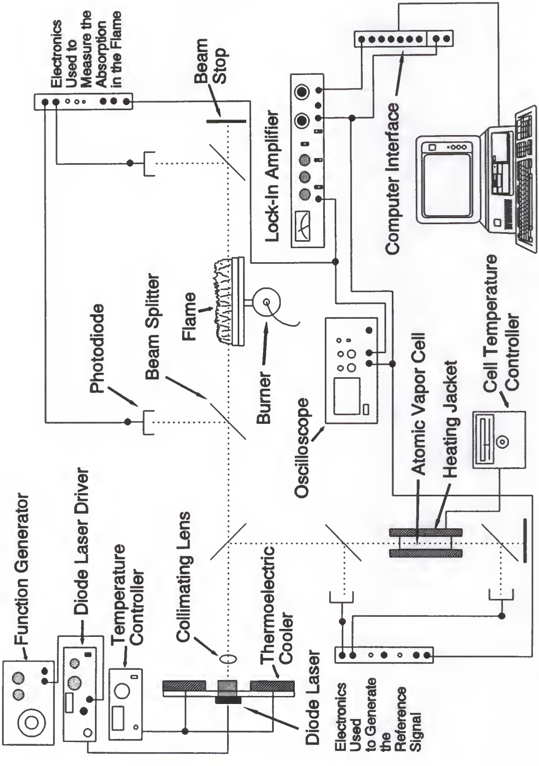
Function Generator
Diode Laser Driver
Temperature Controller
Collimating Lens
Thermoelectric Cooler
Diode Laser
Electronics Used to Generate the Reference Signal
Photodiode
Beam Splitter
Flame
Burner
Oscilloscope
Atomic Vapor Cell
Heating Jacket
Cell Temperature Controller
Beam Stop
Electronics Used to Measure the Absorption in the Flame
Lock-In Amplifier
Computer Interface

Figure 4-2. Drawing Showing a Sinusoidal Modulation Ramp. The Ramp is Superimposed on Top of the Base Driving. In On/Off Modulation, the Laser is Modulated Onto Only Part of the Absorption Profile. In Across Modulation, the Laser is Modulated Across the Entire Absorption Profile.

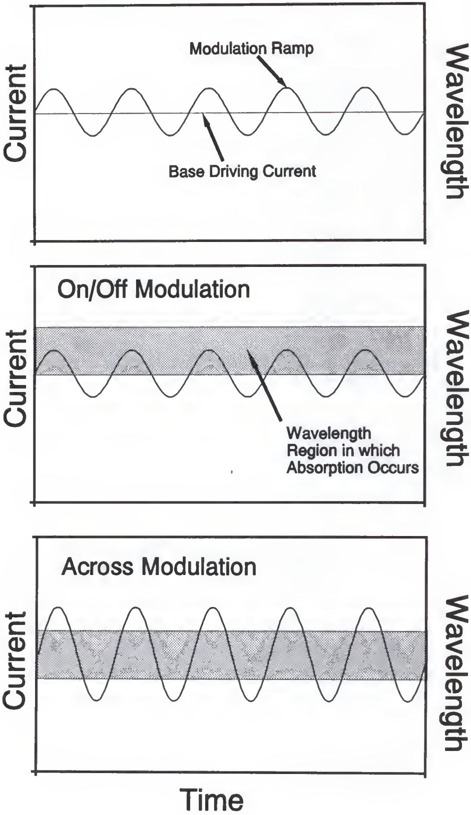
Modulation Ramp
Base Driving Current
Current
Wavelength
On/Off Modulation
Wavelength Region in which Absorption Occurs
Current
Wavelength
Across Modulation
Current
Wavelength
Time

from the instrumentation amplifier. In all measurements, the base line voltage was set to zero.

Although the diode lasers used are specified as being single mode, each diode laser has its own characteristic spectral line structure, which is dependent on the specific current/temperature combination that is used and upon the modulation amplitude. In order to select a diode laser which could be tuned to the 780.023 nm transition of rubidium, the emission of the laser was observed on a F/8.6 Spex 1870 0.5 m Czerny-Turner monochromator onto which a intensity field photodiode array was mounted. Rubidium emission from an air/hydrogen flame was used to calibrate the photodiode array. Various current/temperature combinations were evaluated to tune the frequency of the laser near the resonance wavelength of Rb.

The laser was then tuned to the rubidium resonance by varying the current and temperature while observing the absorption in the vapor cell on an oscilloscope. The rubidium absorption would appear as peaks on the oscilloscope trace when the laser was scanned across the resonance. Once the operating conditions were determined, the laser could be tuned to the transition without the use of the spectrometer. The oscilloscope traces are shown in Figure 4-3. These atomic absorption peaks are produced by the change in the difference of the voltages produced by the photodiodes. Using a modulated diode laser greatly simplified the tuning of the laser, since a range of wavelengths was covered at each temperature and base current setting.

Figure 4-3. Oscilloscope Traces Showing the Modulation Ramp (Upper Trace), the Absorption Signal (Middle Trace), and the Reference Waveform (Lower Trace).
Timebase 2.00 ms/div
Vertical Sensitivity,
    Upper Trace 50mV/div
    Middle Trace 1.40 V/div
    Lower Trace 5.00 V/div

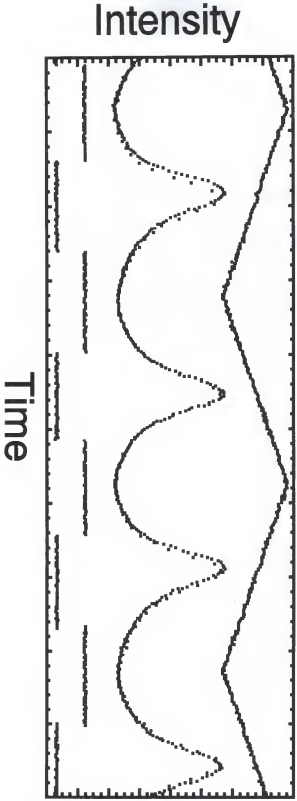
Intensity
Time

Figure 4-4 shows a circuit diagram of the electronics used to generate the reference signal for the lock-in amplifier. The absorption signal measured by the instrumentation amplifier from the vapor cell was converted into a square wave by a LM311 voltage comparator. To avoid multiple triggering of the comparator near the threshold level, feedback through an 18.7 kΩ resistor provided hysteresis. The resulting square wave, lower trace in Figure 4-2, triggered the lock-in amplifier. If the laser wavelength drifted, no phase change occurred between the absorption signal of the flame and the reference signal produced by absorption in the vapor cell. Since the reference follows the laser, this eliminated any noise that would have been produced by using a signal directly from the function generator as the reference. The duty cycle of the absorption was controlled by the amplitude of the modulation ramp.

A 10 cm slot burner supported an air/hydrogen flame. The flow rates were optimized for maximum absorption by observing the output from the lock-in amplifier. The nebulization rate was 10 mL/min with a 20% atomization efficiency. The average driving current of the diode laser was 60 mA. The optimum modulation frequency was found to be 100 Hz. The amplitude of current was 14 mA producing a wavelength modulation of 198 nm. The lock-in amplifier was operated with a time constant of 1.25 s. The standards were prepared from a stock solution of 999 ng/mL AA standard obtained from Aldrich Chemical Company, Milwaukee, WI. The Rb metal vapor cell had a length of 8 cm and a pressure of 100 torr of nitrogen to quench the rubidium fluorescences.

Figure 4-4. Electronic Circuit Used to Shape the Absorption Signal of the Vapor Cell into the Reference Signal. R1, R2, R3, R4, and R5 are 10, 10, 1, 18.7, and 1 kΩ Resistors, Respectively. V_R = Reference Voltage, and Ref is the Reference Output. LM311-voltage comparator. AD524-Instrumentation Amplifier.

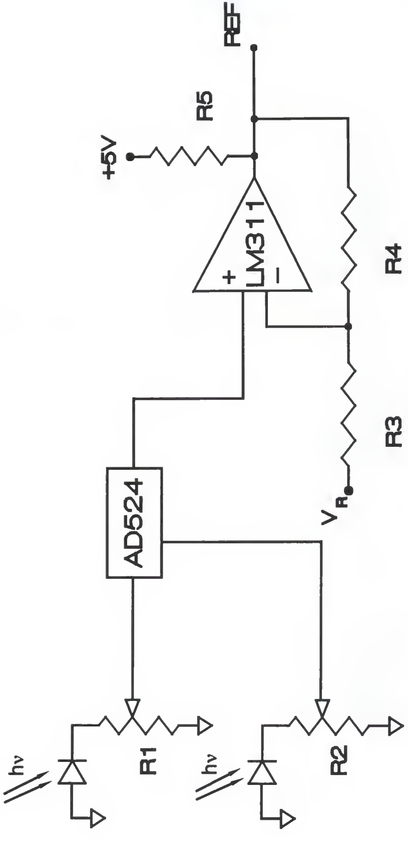
REF
R5
+5V
LM311
+
−
R4
R3
V_R
AD524
hν
R1
hν
R2

Results and Discussion

The quality of the absorption signal is very dependent on the spectral characteristics of the single mode diode laser. It was necessary to try three separate laser diodes before a suitable one was found. The diode laser must be single mode over the entire modulation range and must have a narrow spectral width compared to the absorption line width. If the wavelength modulation is too large, the diode laser will mode hop to another wavelength region. When the laser is operating in a single mode and modulated across the resonance line, an absorption signal as shown in Figure 4-3 is obtained. When the laser is improperly tuned or unstable, the trace would appear as a flat line or as random fluctuations.

Figure 4-5 shows the four different types of modulation that were investigated. The detection limits for rubidium were, respectively, 22, 16, 30, and 10ng/ml for triangular on/off, triangular across, sinusoidal across and sinusoidal on/off modulations. Across refers to when the wavelength of the laser was scanned over (across) the entire transition. On/off refers to when the laser was scanned only over part of the transition, Figure 4-2. These detection limits are over an order of magnitude better than the values reported for a free running diode laser with only temperature stabilization (38) and are comparable to the results obtained with a different type of modulation scheme used by Hergenröder and Niemax (39). A typical conventional AAS detection limit for rubidium in a flame is 5 ng/mL (1). The linear dynamic range was approximately two orders of magnitude for each type of modulation.

Figure 4-5. Different Types of Modulated Signals. Upper Traces Current Modulation Ramp. Lower Traces Absorption Signal.
A triangular on/off,
B sinusoidal on/off,
C triangular across,
D sinusoidal across

Timebase 2.00 ms/div
Sensitivity
Upper traces 60 mV/div
Lower traces 4V/div

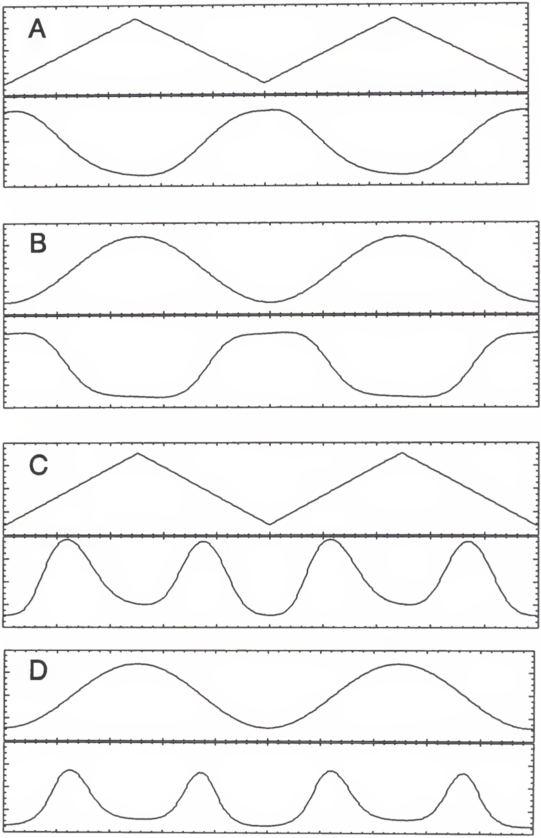
A
B
C
D

The difference in detection limits for the four different types of modulation is too small to draw any definite conclusion about which is better. However, the on/off modulations provides only limited correction for laser variations; as the frequency of the laser drifted, the duty cycle (percentage of time the laser is on the wavelength of the transition) and the effective absorption coefficient either became larger or smaller depending on the direction of shift. If the change is too large, the signal will be completely lost.

The small differences in the detection limits between the different types of modulation may be attributed to the percentage duty cycle which could be obtained by the different types of modulation. Because of the response of the laser to modulation, the sinusoidal on/off modulation which could be adjusted to the highest duty cycle resulted in the lowest detection limit. The same argument follows for modulation across the absorption line. Triangular modulation across the absorption line had a higher duty cycle than sinusoidal across and resulted in better detection limits.

In order to test the effectiveness of the reference generating system, the base driving current of the laser was varied to simulate current or temperature drifts, and a rubidium solution was aspirated into the flame to provide a constant absorption signal. By observing the output from the lock-in amplifier, it was possible to tell if any phase change occurred between the reference signal and the analytical signal. When the wavelength of the laser was varied approximately 15 pm, which is the equivalent to a drift equal to the half width of the absorption profile in the flame, no change in the lock-in amplifiers output was observed for across modulations.

In this study, the diode lasers were observed to age; aging is defined as changes in the emission profile of the laser at a particular current/temperature combination. The rate of aging varied from laser to laser. After a period of use, higher currents were required to tune to the same wavelength. Of the three lasers used in the course of this study, the spectral characteristics of two diode lasers changed so much that they became useless. One of the lasers began to lase multimode and the other laser could not be tuned to the transition after only twenty hours of use. Rapid aging may have been a result of operation above their rated maximum power in order to tune to the rubidium transition. Aging of the diode lasers will definitely limit the development of diode lasers as a source for commercial analytical AAS instrumentation.

Although it was not investigated, this technique should also provide background correction. Any broad band background absorption interference over the entire range of wavelength covered by the modulation will not be detected. The interferent would only change the base level of the voltage produced by the second photodiode monitoring the light intensity after the flame and will therefore not be seen as a time dependent signal by the lock-in amplifier.

CHAPTER 5

DIODE LASER ATOMIC FLUORESCENCE SPECTROSCOPY

Introduction

Atomic Fluorescence Spectroscopy (AFS) offers many analytical advantages compared to AAS including low detection limits, large linear dynamic range, multielement capabilities, simplicity, and freedom from spectral interferences, but there has been little interest in commercialization of an atomic fluorescence spectrometer (1). One of the reasons for this is the lack of reliable, intense, narrow line excitation sources. Since the atomic fluorescence intensity is directly proportional to the excitation source, the ideal source for AFS would be stable and provide very high radiance at the frequency of the atomic transition of interest. The use of dye lasers has made it possible to achieve very low detection limits for a number of elements. Unfortunately, dye laser systems are expensive and require a skilled operator.

Relatively inexpensive diode laser systems could renew interest in the application of AFS. Diode lasers are orders of magnitude more intense than conventional sources such as hollow cathode lamps, and their intensity is more stable than most conventional and laser sources. However, similar difficulties arise when using diode lasers for AFS as when using them for AAS. The same type of approach was used in this work as described in the previous chapter on AAS. In this work, instead of trying to maintain the laser at exactly on the analyte wavelength, the wavelength of the laser was scanned and a reference system was used to generate the reference for a lock-in amplifier (42).

Experimental

The schematic layout of the apparatus used in this study is shown in Figure 5-1. Table 5-1 gives a detailed list of the equipment and experimental conditions. The wavelength tuning procedure described in Chapter 4 was used in the AFS study. The wavelength specified by the manufacturer for the diode laser was 784 nm when operated at 25°C and a current of 40 mA. In order to be tuned to rubidium's most sensitive 780.023 nm absorption, the operating conditions for the laser were 58.40 mA and -4.2 °C. The external modulation signal to the current source was provided by a Wavetek signal generator. The amplitude of the wavelength modulation was 198 pm.

The light emitted from the laser was collimated into an elliptical beam of 5 mm by 1.5 mm. A convex lens of focal length 75 mm focused the laser beam into the center of a air-hydrogen flame. The flame was generated on either an 11 mm or 18 mm diameter circular burner or a 55 mm slot burner set up at an angle of 25° to the laser beam direction. The burner was adjusted to minimize pre- and post-filter effects in the flame. The fluorescence was measured at 90° to the diode laser beam, transferring a 1:1 image with a 75 mm convex lens onto the entrance slit

Table 5-1. Detailed List of the Equipment Used.

DIODE LASER	Mitsubishi ML4402 Power output 3 mW Lasing wavelength (25°C) 780 nm Operating current (25°C) 40 mA
LASER DIODE HOUSING	ILX LIGHTWAVE mod. no. LDM-4412 Operating temperature -4.2 °C
CURRENT SOURCE	ILX LIGHTWAVE mod. no. LDX-3620 Ultra low noise current source
TEMPERATURE CONTROLLER	ILX LIGHTWAVE mod. no. LDT-5910 Temperature controller
MODULATION SOURCE	WAVETEK mod. no. 110 Function generator
NEBULIZER	Perkin Elmer Nebulization rate 10 mL min^{-1} Efficiency 20%
BURNER HEADS	1. Perkin Elmer 55 mm slotted 2. Custom-made circular Diam. 11 mm, 18 mm

Table 5-1. Continued.

FLAME MIXTURE	Hydrogen/air flame Hydrogen = 3.75 L min^{-1} Air auxilliary = 0 Air nebulizing = 5.5 L min^{-1}
LOCK-IN AMPLIFIER	ITHACO Dynatrac mod. no. 391A Frequency range 0.1 - 10 kHz Time constant 1.25 s
OPTICAL REFERENCE UNIT	Rb vapor cell (100 torr nitrogen) Oven heater WEST GAURDSMAN control unit Stabilized temperature 115 °C Diodes: UDT-PIN UV100 487-2
COMPUTER INTERFACE	STANFORD RESEARCH mod. no. SR 245

Figure 5-1. Schematic Diagram of the Apparatus Used for Diode Laser Atomic Fluorescences.

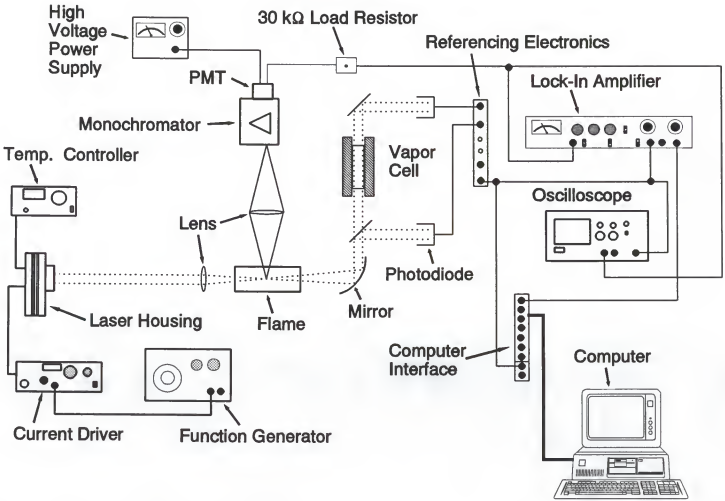
High Voltage Power Supply
30 kΩ Load Resistor
Referencing Electronics
PMT
Lock-In Amplifier
Monochromator
Temp. Controller
Vapor Cell
Oscilloscope
Lens
Photodiode
Laser Housing
Flame
Mirror
Computer Interface
Computer
Current Driver
Function Generator

of an F/3.5 Jobin Yvon H-10 monochromator, oriented on its side so that the 0.5 mm monochromator entrance slit was horizontal to the laser beam allowing a larger solid angle of the fluorescence to be collected. No precautions were taken to baffle the optical path between the focussing lens and the entrance slit of the monochromator to minimize collecting of stray light. The output current of the photomultiplier tube was terminated in a 30 kΩ resistor and displayed on an oscilloscope. The voltage produced by the load resistor was also connected to the input of the lock-in amplifier. The analog output of the lock-in amplifier was digitized and stored by a computer interface.

The diverging diode laser beam after the flame was collimated with a concave mirror and passed through a rubidium vapor cell, the temperature of which was maintained at 115°C. By deflecting part of the laser beam to two identical photodiodes placed before and after the Rb vapor cell, it was possible to generate the reference signal for the lock-in amplifier from the absorption in the vapor cell. The procedure is discussed in detail in Chapter 4. Using this reference eliminated any drift in the output of the fluorescence signal due to phase changes between the reference signal and the fluorescence signal because of random changes in base frequency of the laser.

The energy level diagram in Figure 5-2 shows the rubidium transitions used in this study. Fluorescence was measured at both the resonance and nonresonance wavelengths of 780.023 nm and 794.76 nm, respectively.

Figure 5-2. Energy Level Diagram Showing the Rubidium Transitions Used in This Study.

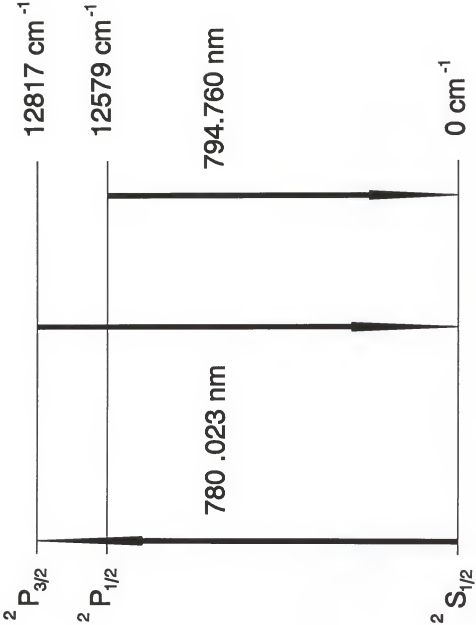
$^2P_{3/2}$
$^2P_{1/2}$
$^2S_{1/2}$
12817 cm $^{-1}$
12579 cm $^{-1}$
0 cm $^{-1}$
794.760 nm
780 .023 nm

Results and Discussion

A comparison between the analytical response of two types of modulation was made. The two modulation approaches were triangular across and sinusoidal on/off. As for the AAS cases, there was no difference between the analytical results obtained for each type of modulation as long as the duty cycles remained the same.

In this study, various burner heads were used. The first test burner was constructed from a number of stainless steel capillary tubes, 1 mm i.d., pressed into an 18 mm brass cylinder. A concentric sheath of argon surrounded the air-hydrogen flame. Since the rubidium transition at 780.023 nm has a large oscillator strength of 0.67, pre-filter and post-filter effects could be observed on the oscilloscope as dips in the center of the fluorescence signal. To minimize these effects, it was necessary to focus the laser beam on the outer edge of the flame on the side toward the monochromator. The linear dynamic range obtained was four orders of magnitude and the detection limit was approximately 1 ng/mL.

In order to increase the number of analyte atoms absorbing in the flame, a smaller circular burner head, 11 mm in diameter, was also used. The linear dynamic range was the same and the detection limit was about the same, 0.8 ng/mL.

Much better results were obtained with a commercial 55 mm slotted burner head. The burner head was placed parallel, 0° orientation, to the laser beam. The beam was focused so as to fill the center of the flame. Because the flame produced by the burner was a long thin rectangle, fluorescence collected perpendicular to the burner had minimum post-filter effects, but pre-filter effects still limited the calibration curve's linearity to four orders of magnitude and the detection limit was still 1 ng/mL. The burner head was then rotated with respect to the diode laser beam to yield the highest fluorescence signal using 1 ng/mL solution of Rb. At a 25° angle, the image of the intersection of the diode laser beam with the flame was exactly equal to the length of the monochromator slit height. The linear dynamic range in this configuration improved to five orders of magnitude. The detection limit for Rb was 0.2 ng/mL, which was better than the 0.4 ng/mL that was previously obtained using a high power multi-longitudinal mode laser with a graphite furnace atomizer (43).

Since the upper levels of the two Rb spectral lines 780.023 and 794.76 nm are only 38 cm^{-1} apart (Figure 2), collisions at atmospheric pressure will result in rapid redistribution between these two levels. Therefore, excitation at 780.023 nm will result in nonresonance fluorescence from the lower level at 794.760 nm. This excitation scheme minimized measured scatter from the laser, but because the transition probability for the 794.760 nm transition is 2.3 times less than that of the 780.023 nm transition, no improvement in detection limit was obtained. The dynamic range was five orders of magnitude but the detection limit was 1.4 ng ml^{-1}. However, this does illustrate the possibility of using collision-connected upper levels for nonresonance fluorescence.

The diode laser was not sufficiently intense to saturate the absorption transition. Ideally a concave mirror could have been placed after the flame to focus back into the flame the non-absorbed laser beam. This would probably have increased the fluorescence from the flame, but because no optical isolator was available to protect the laser against optical feedback, this was not attempted.

In this study, the diode laser was found to be susceptible to mode hops due to optical feedback from scatter off salt particles that sporadically emerged from the burner. When the laser mode hopped, the laser was tuned back to the absorption transition; since the reference always had the same phase relationship to the fluorescence signal, adjustments of the lock-in amplifier were not needed to reproduce the signal. It should be emphasized that the use of a clean burner is required and the current/temperature combination of the diode laser should not be near a mode hop.

CHAPTER 6

EVALUATION OF ABSOLUTE NUMBER DENSITIES BY DIODE LASER ATOMIC SPECTROSCOPY

Introduction

The goal of many atomic spectroscopists has been to develop a standardless method in which the concentration of an analyte in an unknown matrix could be determined without the use of a calibration curve (44). A standardless technique requires knowledge of both the atomization efficiency and factors which affect the measurement of the analyte in the vapor phase. A variety of atomizers have been suggested for use in standardless analysis. Some of the atomizers include flames, plasmas, vapor cells, and graphite furnaces (21, 45-48). The benefits and problems associated with their use has been extensively reviewed and will not be discussed here, but it should be mentioned that graphite furnaces are being developed which are approaching freedom from matrix effects and have well characterized atom and temperature distribution (46).

Once the analyte has been atomized, numerous techniques have been used to measure the absolute number density (49,50). Most of these methods are based on the measurement of atomic emission, atomic absorption, or atomic fluorescence. Many absolute methods depend on accurate calibration of the detection optics and photodetection. For example, in atomic emission or atomic fluorescence, it is also necessary to know the spectral responsivity and gain of the detector and associated electronics, and the efficiency and throughput of the optics. Emission techniques are hindered by the need for a well characterized excitation source. A 1% error in the measurement of the temperature of excitation can result in errors greater than 10% in the calculated number density (21). Almost all procedures used for absolute analysis require knowledge of the absorption oscillator strength and spectral profile of the analyte transition being studied.

One of the oldest methods of estimating the absolute number density is the integral-absorption method. In this approach, the absorption factor is normally measured with a continuum source such as a tungsten strip or xenon arc. The absorption factor is measured over the entire profile by setting a monochromator at the central frequency of the absorption and using large enough slit widths so that the bandpass is greater than the line width. It is usually assumed that the spectral output of the source is constant over the bandpass. At low optical densities, the absorption factor for a continuum source unlike peak absorption with a line source, is independent of the absorption profile. The absorption factor, α_c, with a continuum source can be written as

$$\begin{aligned} \alpha_c &= \frac{I_a(\lambda)}{I_t(\lambda)} \\ &= \frac{\pi e^2 \ell \lambda_o^2 n_a f}{mc^2 \Delta\lambda_s} \end{aligned} \qquad 6\text{-}1$$

where $\Delta\lambda_s$ is the bandpass of the monochromator (cm), ℓ is the pathlength of the absorption (cm), λ_o is the central wavelength of absorption, n_a is the number of absorbing atoms, f is the oscillator strength (dimensionless), m is the electron mass (g), and c is the velocity of light (cm s^{-1}). The absorption factor is related to the integral absorption, A_T, by

$$\alpha_c = \frac{A_T}{\Delta\lambda_s} \tag{6-2}$$

where A_T has units of cm. At high optical densities, the absorption factor is related to number densities through the expression

$$\alpha_c = \frac{1}{\Delta\lambda_s}\sqrt{\left(\frac{2\pi e^2}{mc^2}\right)\ell\lambda_o^2 n_a f \Delta\lambda_{eff}} \tag{6-3}$$

where $\Delta\lambda_{eff}$ is the overall line profile of the atomic transition.

Two of the problems with using integral absorption for evaluating number densities is that the oscillator strength of the transition must be known and the bandpass of the monochromator must be accurately calibrated. Another approach to absolute analysis is to make relative measurements of two signals. In the case of integral absorption, the absorption factor is measured for a known α_1 and for an unknown α_2. By taking the ratio of the two absorption factors, it is found that

$$\frac{\alpha_1}{\alpha_2} = \frac{n_1\ell_1}{n_2\ell_2} \tag{6-4}$$

This relative measurement does not require either the bandwidth of the monochromator or the absorption oscillator strength, and allows the unknown n_2 to be calculated from the known n_1 number density.

In this work, a new method for evaluation of absolute number densities has been investigated. It is based on measuring the absorption factor with a diode laser. By making relative measurements of the absorption from a well characterized reference cell and an analytical cell, it is possible to estimate the number density of the analytical cell from the number density of the reference cell (51).

Theory

Schematics and terminology for the three proposed experimental setups are given in Figures 6-1. Table 6-1 gives the relationships of the photodiode signals to the intensity of the laser. The analytical atom source or cell will be referred to as being either on or off. The term off will refer to the case when a blank is being atomized. On refers to the case when a sample containing the analyte is being atomized. The analytical cell could be any type of atomizer. The reference cell is an atomic vapor cell which contains rubidium metal and nitrogen to quench fluorescence. When the vapor cell is uniformly heated and at equilibrium, the number density of rubidium can be calculated from the vapor pressure of the metal. Using the above terminology, the reference cell is always on.

Since the spectral band width of a diode laser is much narrower than the band width of the atomic absorption, the absorption signal generated by scanning the wavelength of the laser across the transition gives the absorption profile of the atomic transition. By definition, the area of the absorption profile is proportional to the integral absorption. Thus, by measuring the absorption as a function of

Figure 6-1. Schematics and Terminology for the Three Proposed Experimental Arrangements.

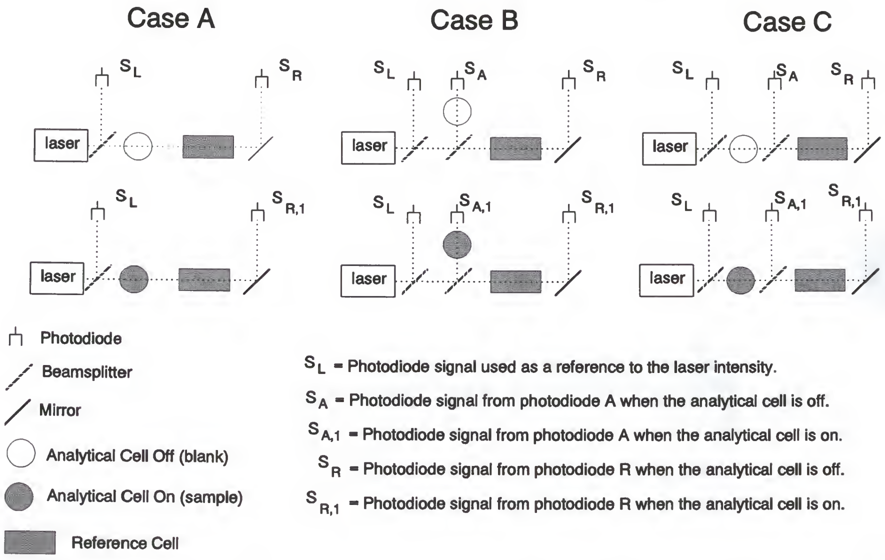

S_L = Photodiode signal used as a reference to the laser intensity.

S_A = Photodiode signal from photodiode A when the analytical cell is off.

$S_{A,1}$ = Photodiode signal from photodiode A when the analytical cell is on.

S_R = Photodiode signal from photodiode R when the analytical cell is off.

$S_{R,1}$ = Photodiode signal from photodiode R when the analytical cell is on.

Table 6-1. Relationship of Photodiode Signal to the Integrated Intensity of the Laser Beam.

$$S_L = \int_{\Delta\lambda_s} I_\ell(\lambda) d\lambda$$

$$S_A = \int_{\Delta\lambda_s} I_\ell(\lambda) d\lambda$$

$$S_R = \int_{\Delta\lambda_s} I_\ell(\lambda) e^{-k_R(\lambda)\ell_R} d\lambda$$

$$S_{A,1} = \int_{\Delta\lambda_s} I_\ell(\lambda) e^{-k_A(\lambda)\ell_A} d\lambda$$

$$S_{R,1} = \int_{\Delta\lambda_s} I_\ell(\lambda) e^{-k_A(\lambda)\ell_A} e^{-k_R(\lambda)\ell_R} d\lambda$$

$$R_L = \frac{S_L}{S_L}$$

$$R_A = \frac{S_A}{S_L}$$

$$R_R = \frac{S_R}{S_L}$$

$$R_{A,1} = \frac{S_{A,1}}{S_L}$$

$$R_{R,1} = \frac{S_{R,1}}{S_L}$$

$I_\ell(\lambda)$ - Intensity of the laser (mW); $\Delta\lambda_s$ - Wavelength range over which the signal is integrated; $k(\lambda)$ - Absorption coefficient (cm^{-1}); ℓ - pathlength (cm) wavelength or of the scan time, the diode laser acts as a continuum source in time with a bandpass equivalent to the range of the scan. This can easily be measured using an oscilloscope.

Case A

In this arrangement, Figure 6-1, both the analytical and reference cells are placed along the same optical path of the laser. The absorption of the reference cell is first measured when the analytical cell is off. The area of the oscilloscope trace obtained can be described by

$$\begin{aligned}\mathrm{Area}_{\mathrm{Off}} &\equiv R_L - R_R \\ &\equiv \frac{S_L}{S_L} - \frac{S_R}{S_L} \\ &\equiv \frac{S_L - S_R}{S_L} \\ &\equiv \frac{\int_{\Delta\lambda_S} I_\ell(\lambda)d\lambda - \int_{\Delta\lambda S} I_\ell(\lambda)e^{-k_R(\lambda)\ell_R}d\lambda}{\int_{\Delta\lambda S} I_\ell(\lambda)d\lambda} \\ &\equiv \alpha_R\end{aligned} \qquad 6\text{-}5$$

assuming the scan of the laser encompasses the entire absorption profile. α_R is the absorption factor of the reference cell. The area of the oscilloscope trace is then measured when the analytical cell is on so that

$$\mathrm{Area}_{\mathrm{On}} \equiv R_L - R_{R,1} \equiv \alpha_A + \alpha_R \qquad 6\text{-}6$$

where α_A is the absorption factor of the analytical cell. If both cells are optically thin and the summation of their absorption does not exceed optically thin conditions, the areas measured can be related to the number densities by

$$\mathrm{Area}_{\mathrm{Off}} \equiv \left(\frac{\pi e^2 \lambda_o^2 f}{mc^2}\right) n_R \ell_R \qquad 6\text{-}7$$

and

$$\mathrm{Area}_{\mathrm{On}} \equiv \left(\frac{\pi e^2 \lambda_o^2 f}{mc^2}\right) (n_A \ell_A + n_R \ell_R) \qquad 6\text{-}8$$

By taking the ratio of the areas, it is found that

$$\frac{\mathrm{Area}_{\mathrm{On}}}{\mathrm{Area}_{\mathrm{Off}}} \equiv \frac{n_A \ell_A + n_R \ell_R}{n_R \ell_R} \qquad 6\text{-}9$$

Thus, if the number density of the reference cell is known, the number density of the analytical cell can be calculated without knowledge of the absorption oscillator strength. Since the same optics and detection system is used for both the reference and analytical measures, any instrumental factors will cancel. When the absorption in the cells exceed optically thin conditions, no general expression can be derived to relate the area to the number density.

Case B

Case B considers the absorption of the analytical cell and reference cell in the optical arrangement shown in Figure 6-1B. This case differs from Case A in that the absorption cell and the reference cell are placed in separate optical paths. Since different optics and electronics are used for the reference cell and the analytical cell, Case B requires accurate calibration of both detection paths. The reference area is

$$\text{Area}_{\text{Off}} \equiv R_L - R_R \equiv \alpha_R \tag{6-10}$$

and the analytical area from the other optical path

$$\text{Area}_{\text{On}} \equiv R_L - R_{A,1} \equiv \alpha_A \tag{6-11}$$

Under optically thin conditions, the ratio of the areas gives

$$\frac{\text{Area}_{\text{On}}}{\text{Area}_{\text{Off}}} \equiv \frac{n_A \ell_A}{n_R \ell_R} \tag{6-12}$$

Assuming that the instrumental factors are the same for both the reference and the analytical measurement. When both cells are optically thick,

$$\frac{\text{Area}_{\text{On}}}{\text{Area}_{\text{Off}}} \equiv \frac{\sqrt{n_A \ell_A \Delta \lambda_{L,A}}}{\sqrt{n_R \ell_R \Delta \lambda_{L,R}}} \tag{6-13}$$

In this situation, it is necessary to know the Lorentzian half-width, $\Delta\lambda_L$ for the analyte in the analytical A and the reference R cells.

Case C

In this arrangement, the difference, D, between the ratios of S_A and S_R to S_L is measured.

$$D_{\text{OFF}} \equiv \frac{S_A}{S_L} - \frac{S_R}{S_L} \tag{6-14}$$

$$D_{\text{On}} \equiv \frac{S_{A,1}}{S_L} - \frac{R_{R,1}}{S_L} \tag{6-15}$$

Since the ratio of the photodiode signals is taken, it is assumed that the intensity of the laser as measured by the ratio is independent of wavelength.

When the analytical cell is off, D_{Off} is given by

$$D_{Off} \equiv \int_{\Delta\lambda_s} (1 - e^{-k_R(\lambda)\ell_R}) d\lambda \qquad 6\text{-}16$$

and when the analytical cell is on, D_{On} is given by

$$D_{On} \equiv \int_{\Delta\lambda_s} e^{-k_A(\lambda)\ell_A} (1 - e^{-k_R(\lambda)\ell_R}) d\lambda \qquad 6\text{-}17$$

To calibrate the system, D_{Off} is measured, when the reference cell is optically thin, $k_R(\lambda)\ell_R << 1$, and the analytical cell is Off, so that

$$D_{Off} \equiv \int_{\Delta\lambda_s} k_R(\lambda)\ell_R d\lambda \qquad 6\text{-}18$$

The difference between D_{Off} and D_{On} is designated D' and is defined as

$$\begin{aligned} D' &\equiv D_{Off} - D_{On} \\ &\equiv \int_{\Delta\lambda_s} (1 - e^{-k_A(\lambda)\ell_A})(1 - e^{-k_R(\lambda)\ell_R}) d\lambda \end{aligned} \qquad 6\text{-}19$$

The analytical measurement is made by measuring the D' when the reference cell is optically thick $k_R(\lambda)\ell_R >> 1$ and the analytical cell is optically thin, the difference D' is then

$$D' \equiv \int_{\Delta\lambda_s} k_A(\lambda)\ell_A d\lambda \qquad 6\text{-}20$$

Figure 6-2 depicts how the absorption in the analytical cell effects of the difference measured between photodiodes R_A and R_R. R_A and R_R are shown in A and B. When the analytical cell is off, the difference, D_{Off}, between the two

Figure 6-2. Graphical Depiction of D_{Off} and D_{On}.

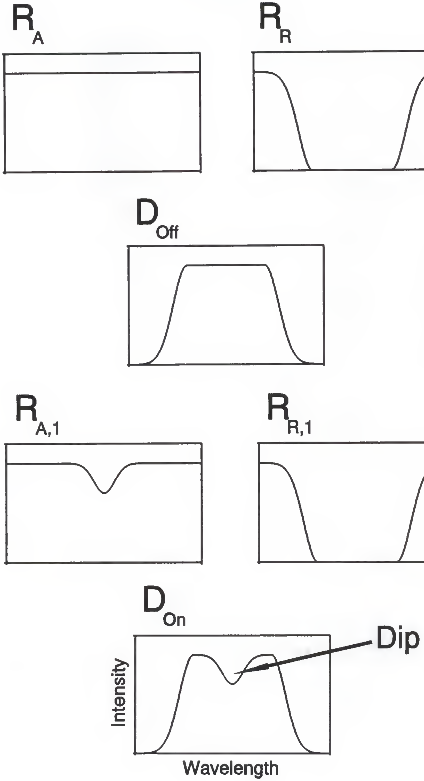
R_A
R_R
D_{Off}
$R_{A,1}$
$R_{R,1}$
D_{On}
Dip
Intensity
Wavelength

photodiodes is shown in C. By introducing the analyte into the analytical cell, the first photodiode, $R_{A,1}$, will detect the absorption of the analytical cell. Since the reference cell is optically thick no light is transmitted in the central portion of the line so that the absorption in the analytical cell is not observed by the second photodiode, $R_{R,1}$. When the difference is taken between $R_{A,1}$ and $R_{R,1}$, the absorption in the analytical cell is superimposed upon the absorption of the reference. This appears as a dip in the reference cell absorption.

By taking the ratio of D′ and D_{Off}, and using the relationship. Eq. 3-2,

$$\int_{\Delta\lambda_a} k(\lambda)d\lambda \equiv \frac{\pi e^2 \lambda_o^2}{mc^2} fn \tag{6-21}$$

it is found that

$$\frac{D'}{D_{Off}} \equiv \frac{n_A \ell_A}{n_R \ell_R} \tag{6-22}$$

Experimental

Figures 6-3 and 6-4 show in detail the experimental set ups for Case A and Case C. Because of the lack of availability of instrumentation, Case B was not evaluated. The laser diode driver, housing, and temperature controller are the same as used in Chapter 3 and 4. Equipment which is different than previously used is listed in Table 6-2. The flux of laser light reaching the photodiodes was controlled using an iris placed before each photodiode. The iris was opened or closed to attenuate the amount of light passing to the photodiode so that identical response

Figure 6-3. Detail Drawing of the Experimental Set up Used to Study Case A.

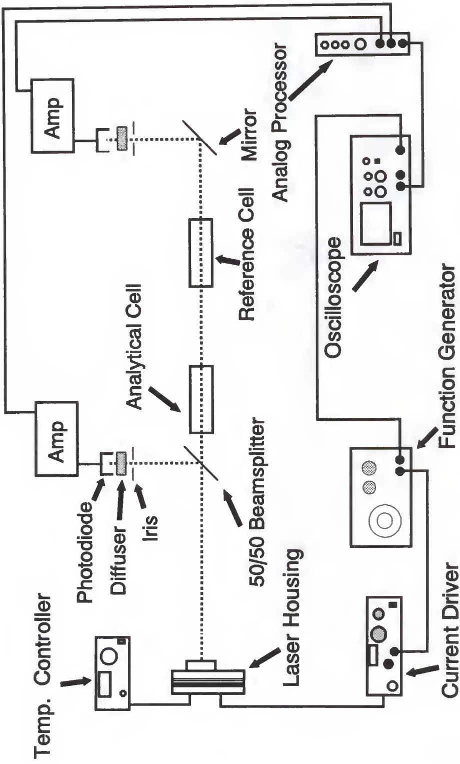
Temp. Controller
Photodiode
Diffuser
Iris
Amp
50/50 Beamsplitter
Laser Housing
Analytical Cell
Reference Cell
Mirror
Amp
Analog Processor
Oscilloscope
Function Generator
Current Driver

Figure 6-4. Detail Drawing of the Experimental Set up Used to Study Case C.

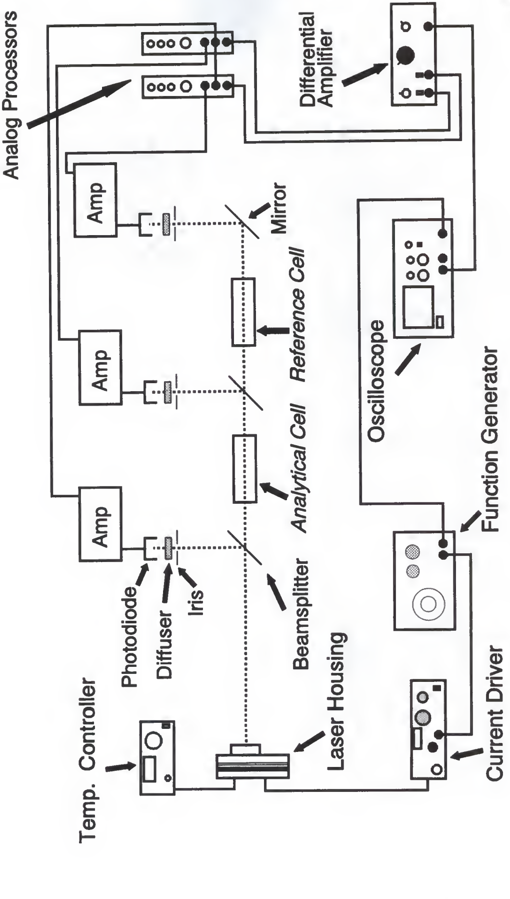
Temp. Controller
Laser Housing
Current Driver
Photodiode
Diffuser
Iris
Beamsplitter
Amp
Analytical Cell
Amp
Reference Cell
Amp
Mirror
Function Generator
Oscilloscope
Analog Processors
Differential Amplifier

Table 6-2. Partial List of Equipment Used for Absolute AAS (See Table 4-1 for Other Equipment).

Pre-Amp	Model 113 Princeton Applied Research, Princeton, New Jersey
Function Generator	FG501A 2 MHz Tektronix, Inc., Beaverton, Oregon
Oscilloscope	2232 100 MHz Digital Storage Oscilloscope, Tektronix, Inc., Beaverton, Oregon

to the modulated laser intensity could be obtained. Opal glass diffusers were placed directly in front of the photodiodes to reduce the effects caused by movement ofthe laser beam with respect to the active area of the photodiode surface. The current produced by the photodiodes was terminated in a 50Ω load resistor. The voltage produced was amplified using a pre-amplifier with a gain of 10^3 and a 3dB low pass filter was set at 30 kHz. A Stanford analog processor was used to take the ratio of the photodiode signals. The output of the analog processor was connected to a Tektronix 2232 digital storage oscilloscope. The oscilloscope traces of the absorption signals were transferred to an IBM computer using a small routine written in BASIC. The data was then stored and processed using Quattro Pro® from Borland International, Inc.

To avoid any distortion of the integral absorption signal due to slight differences between the photodiodes, the temporal response of the photodiodes was measured. The photodiodes were terminated in a 50Ω load resistor and mounted in the same orientation. The response of the photodiodes to the modulated intensity of the laser was recorded by an oscilloscope. Photodiodes with the most similar responses were used. It should be stressed that it was extremely important to match the responses of the photodiodes since optically thin conditions produced very small changes in the current of the photodiodes.

Due to the reflections off the vapor cell's window, constructive and destructive interference could be observed when the wavelength of the laser was scanned. To minimize the amplitude of the interference fringes, the vapor cell was rotated slightly with respect to the laser beam. It was also necessary to use cube beam splitters which produced little noise due to interference.

The temperature of the vapor cell was controlled by a custom-made water jacket. A diagram of the water jacket is given in Figure 6-5. Water from a temperature controlled bath was pumped through copper tubing forming coils which were lead soldered to a copper tube surrounding an aluminum sleeve which was machined to approximately 0.050" larger than the diameter of the vapor cell. Thermal grease was used to ensure good heat transfer between the copper-aluminum and aluminum-glass interfaces. The water temperature was controlled to within 0.1°C. If it was desired to cool the vapor cell, ice water was pumped through a copper coil submersed in the bath.

The temperature of the cell was measured by placing a K-type thermocouple into a hole drilled into the jacket. To ensure that the cell was uniformly heated, the temperature was tested in several places. The cell temperature could be regulated to within 0.1°C. Whenever the temperature of the vapor cell was increased or decreased, at least ten minutes were required for every 0.3°C temperature change before the measured cell temperature stabilized.

Results and Discussion

A fundamental assumption of this work is that the number density in the vapor cell can be calculated from the vapor pressure (52). Therefore, this requires that the temperature of the cell be highly regulated and that equilibrium is

Figure 6-5. Water Jacket Used to Control Cell Temperature.

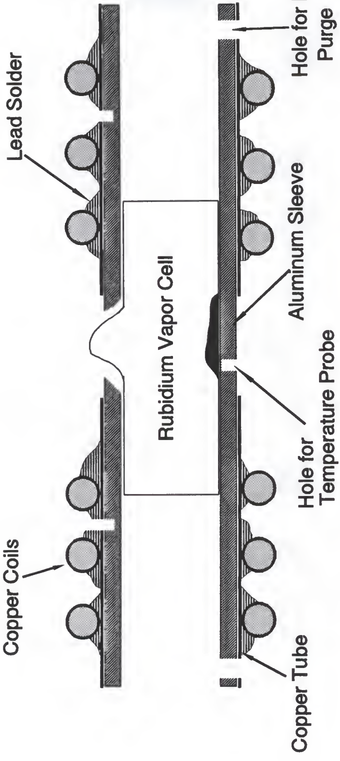
Copper Coils
Lead Solder
Rubidium Vapor Cell
Copper Tube
Hole for Temperature Probe
Aluminum Sleeve
Hole for Nitrogen Purge

established between the gas and solid or liquid phases of the metal. This may not be a valid assumption since the windows of the cell may be slightly cooler or warmer than the sides of the cell, and rubidium which was studied in this work reacts with the glass of the cell walls and windows. However, within the precision of this work once the cell was maintained at the same temperature for at least ten minutes the absorption signal would remain constant as long as the cell temperature was held constant.

Because laser diodes and photodiodes have low noise, it is possible to measure very small absorptions. The three traces in Figure 6-6 show the excellent signal to noise ratio which can be obtained with diode lasers. The upper and lower traces are 100% and 0% transmittance, respectively. These traces are on a 2V scale. The middle trace on a 5mV scale shows the absorption measured in a vapor cell at 14.4°C corresponding to a number density of 9.3×10^9 cm^{-3} (52). The absorption factor can be calculated by dividing the area of the absorption trace by the area between 0% and 100% transmittance. The absorption factor in this figure is approximately 10^{-4}. The linear relationship between the absorption factor and number density is shown in Figure 6-7.

The integral absorption of rubidium was measured in a flame. A linear relationship was found between the absorption factor and Rb number density over a linear dynamic range of two orders of magnitude. The detection limit was 8 ng/ml.

Figure 6-6. Rubidium Absorption in a Vapor Cell at 14.4 °C. The 100% and 0% T Traces are on the Scale of the Primary Axis (Left). The Absorption is on the Scale the Secondary Axis (Right).

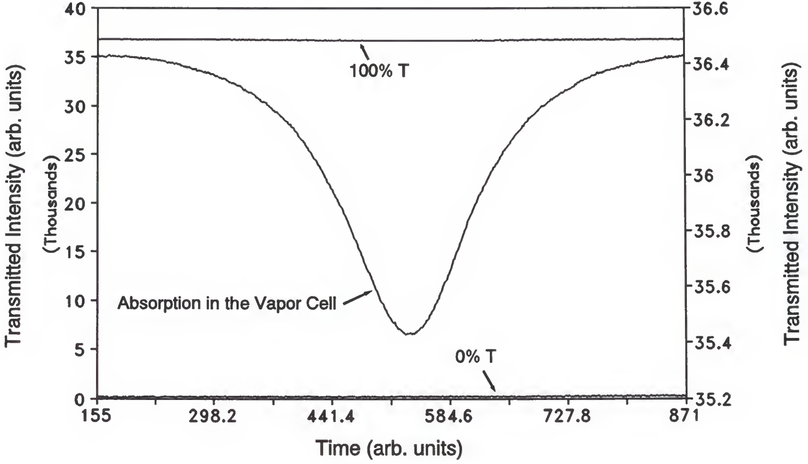
40
35
30
25
20
15
10
5
0
Transmitted Intensity (arb. units)
(Thousands)
36.6
36.4
36.2
36
35.8
35.6
35.4
35.2
Transmitted Intensity (arb. units)
(Thousands)
100% T
Absorption in the Vapor Cell
0% T
155
298.2
441.4
584.6
727.8
871
Time (arb. units)

Figure 6-7. Plot of Absorption Factor Versus Rubidium Number Density.

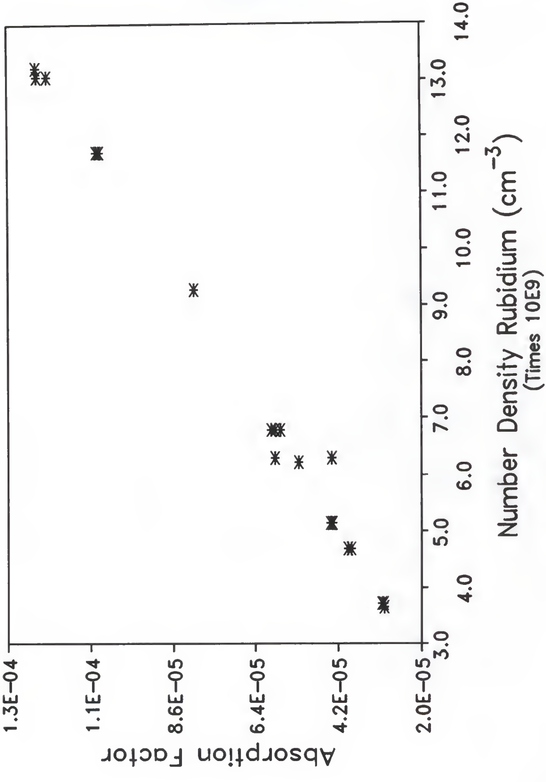
Absorption Factor
1.3E-04
1.1E-04
8.6E-05
6.4E-05
4.2E-05
2.0E-05
3.0
4.0
5.0
6.0
7.0
8.0
9.0
10.0
11.0
12.0
13.0
14.0
Number Density Rubidium (cm⁻³)
(Times 10E9)

An attempt was made to verify the relationship in Case A. Two vapor cells were housed in water cooling jackets. One of the vapor cells was mounted on a X-Y translational platform similar to one used for milling metal. The platform could be positioned to approximately one thousandth of an inch. One cell was cooled to 283 K and the temperature of the cell that was mounted on the platform was varied from 273 K to 290 K. By moving the cell on the platform, it was hoped this would stimulate an analytical cell with on/off type of behavior. When the vapor cell was removed from the optical path of the laser, an empty pyrex cell was moved into the path of the beam to compensate for losses due to reflections off the windows. Unfortunately, the experiment did not give satisfactory results. The precision of the experiment was severely limited by changes in the interference pattern produced by the windows of the cell each time the cell was placed into the optical path. The reason for its failure was that the cell could not be repositioned accurately enough to avoid changes in the interference pattern produced by the windows of the cell. The calculated Rb number density for the moveable vapor cell was approximately 0.5 to 1.2 of the predicted number density.

The modulation amplitude of the laser used in this study could not exceed 70 pm. Since the absorption profile for an optically thick vapor cell is greater than 80 pm wide, it was not possible to measure the integral absorption. This prevented the verification of the theory calculated for Case C. However, it was possible to observe the absorption of a Rb flame superimposed on the absorption of an optically thick vapor cell. When the concentration of the solutions aspirated into the flame was increased systematically, an increase in the size of the absorption dip was observed, as shown in Figure 6-8.

Figure 6-8. Oscilloscope Trace Showing the Absorption of the Flame Superimposed on the Absorption of the Vapor Cell. The Concentrations of Rb Aspirated into the Flame were A 0 ppm, B 10 ppm, C 20 ppm, D 40 ppm, and E 60 ppm.

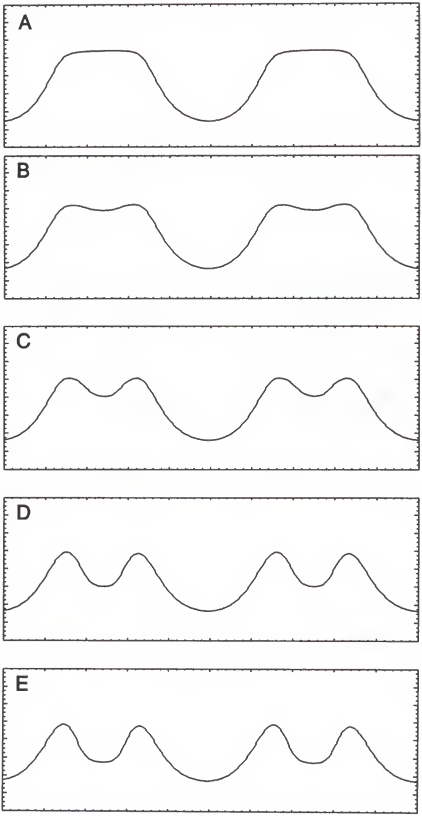
A
B
C
D
E

CHAPTER 7

CONCLUSIONS

Semiconductor diode lasers can be used as the primary source for atomic absorption and atomic fluorescence spectroscopy. Diode lasers offer many advantages over other types of tunable laser systems. For routine analysis, the most important advantages of a diode laser are its low cost and ease of operation while still providing a narrow spectral line width, tunable, and intense source. In this work, it has been demonstrated that diode lasers can be used to measure both peak and integral absorption. Since diode lasers can be used to measure the hyperfine structure of an atomic transition (see Appendix), there is the possibility of using diode lasers for isotopic analysis. The detection could be optical or the laser could be used to ionize an atom providing a selective ion source for mass spectrometry.

Although diode lasers have many advantages over other tunable lasers and conventional sources, there are several difficulties associated with their use. Many of these problems, such as optical feedback causing changes in the emission of the laser, can be solved by proper experimental design. The main disadvantage of commercially available diode lasers is associated with wavelength tuning of the laser. Mode hopping makes it extremely difficult to find a diode laser which can be tuned to the desired wavelength. Diode lasers will not be widely, or if at all, used for analytical atomic spectroscopy until a method is developed which allows the laser to be easily and quickly tuned to the atomic transition without the use of expensive spectrum analyzers.

Feedback from external optics can be used to force the laser to lase at the desired frequency and to eliminate mode hops. Gratings and Fabry-Perot interferometers have been used to select the wavelength which is reflected back into the laser in order to cause it to lase at the desired wavelength. Although this greatly improves the emission characteristics and tunability of the laser, the addition of external optics requires proper alignment making their use in most cases rather complex. Since the potential market of analytical and physical spectroscopy is nonexistent compared to the overall diode laser market, it is reasonable to expect diode laser manufacturers will consider making diode lasers which lase only at wavelengths which are of use for analytical atomic spectroscopy.

The other major limitation to the application of diode laser to analytical spectroscopy is the limited wavelength coverage of currently available commercial diode lasers. The lowest available wavelength from a commercially available diode laser is 620 nm. This severely limits the number of elements which can be studied. Research laboratories have obtained lasing at blue wavelengths. Therefore, if the problems associated with growing these types of semiconductor materials are solved, laser diodes which lase at much shorter wavelengths may become available in the near future.

At the present time, it may be advantageous frequency doubling of the wavelength emitted from the diode laser to make it possible to analyze a greater number of elements. There two approaches which could be taken are frequency doubling using a doubling crystal or using the second harmonic emitted from the diode laser. Frequency double diode systems using doubling crystals and commercially available diode lasers are now available from several commercial sources. These systems are advertised as emitting several microwatts of power. Unfortunately, they have a very small tuning range due to the phase matching angle of the doubling crystal. Manufacturers may be willing to match diode lasers with the proper alignment of the doubling crystal to provide the required wavelength, but special arrangements and guarantees should be made before purchasing to ensure that the desired wavelength will be obtainable.

Since the semiconductor material used to construct diode lasers is a nonlinear crystal, diode lasers emit a natural second harmonic of their fundamental wavelength (29). The power of the second harmonic output is usually, and unfortunately, only a picowatt or less, but this sufficient power to observe atomic absorption.

APPENDIX

QUALITATIVE COMPARISON OF THE SPECTRAL PROFILE OF A RUBIDIUM HOLLOW CATHODE LAMP AND RUBIDIUM ABSORPTION IN A FLAME

In his classic paper, Walsh proposed several simplifying assumptions for measuring peak absorption with a hollow cathode lamp, HCL (53). First, the emission line profile of the HCL is assumed to be much narrower than the absorption line profile in the flame. Therefore, the HCL output is considered monochromatic. Second, collisional shifting of the absorption and emission frequency is ignored so that the frequency of the absorption maximum is considered to be at the same frequency as the emission from the HCL. It is also assumed that the absorption line profile is determined only by the Doppler and lifetime broadening. This allows the absorption coefficient to be expressed by the Voigt profile.

While these assumptions are valid in a number of cases, they do not hold for all elements. The influence of spectral line profiles has been studied in detail by Wagenaar (54). The emission profile from a HCL in many cases can not be considered a line source due to broadening mechanisms. It is also not valid in some cases to consider that the peak emission and the peak absorption occur at the same wavelength. The direction and amount of shift depends on the pressure of the foreign gas and its collisional cross section. Since most atomic transitions have some hyperfine structure, it is not always valid to assume the Voigt profile will describe the absorption coefficient.

Because the spectral line profile of a diode laser is typically less than 20 MHz, it is possible to use a diode laser to study the hyperfine structure and the line profile of an atomic transition (13,17,34). This can be performed by frequency scanning the frequency of the laser across the atomic absorption line. By observing the atomic absorption or atomic fluorescence signal, it is possible to determine the line profile.

Experimental

The experimental equipment and operating conditions are listed in Table A-1. In the absorption experiment, Figure A-1, the emission for the laser was collimated into an elliptical beam of 5 mm by 1.5 mm. The beam was directed between the anode and cathode of the HCL, and the absorption was measured using photodiodes as previously discussed. The spectra were recorded with a digitizing oscilloscope.

In order to compare the absorption profile of a flame to a hollow cathode lamp, the laser beam was split 50/50 and part of the beam was directed in the HCL, Figure A-2, and part was focussed into the flame. The beam was expanded before the beam splitter with an anamorphic prism pair to give a beam of approximately 5 mm in diameter. This allowed the beam to completely fill the cathode of the HCL. The fluorescence signal was collected at a 90° angle to the laser beam in both

Table A-1. Experimental Equipment for Measurement of Hyperfine Structure of Rb in a Hollow Cathode Lamp and a Flame.

Flame	Hydrogen/Air 55 mm slot burner head Perkin Elmer Premix Burner
Hollow cathode lamp	Rubidium 5 torr Ne Fisher Scientific Heath Model EN-703-62 Power Supply 0-10 mA operating current
Monochromator - HCL	Spex Minimate 0.22 m monochromator slits 0.25 mm PMT R955 at 1000 V
Monochromator - flame	Jobin Yvon H-10 100 mm monochromator slits 0.25 mm PMT R1457 at 100V
Laser diode	Same as listed in Table 4-1. Current laser 54.93 mA Temperature 11.0°C Modulation 60 to 80 pm

Figure A-1. Experimental Arrangement Used to Measure Absorption in an Hollow Cathode Lamp.

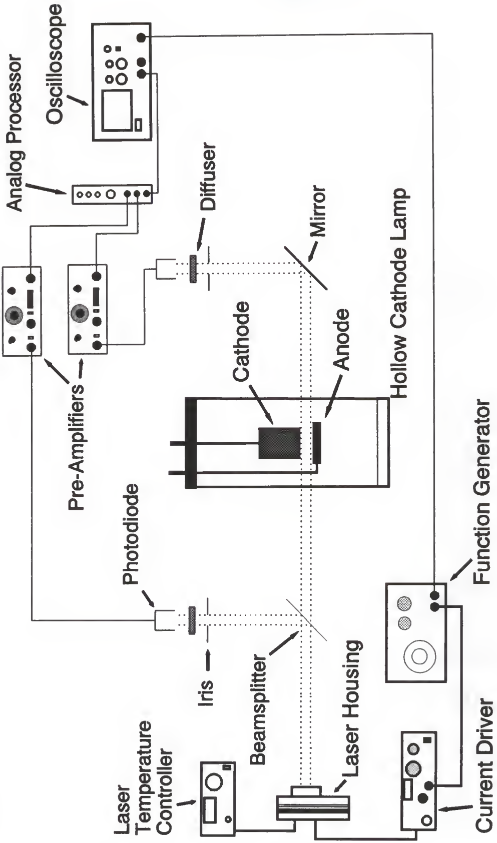
Laser Temperature Controller
Laser Housing
Current Driver
Beamsplitter
Iris
Photodiode
Function Generator
Pre-Amplifiers
Cathode
Anode
Hollow Cathode Lamp
Mirror
Diffuser
Analog Processor
Oscilloscope

Figure A-2. Experimental Lay Out to Measure Atomic Fluorescence Simultaneously in the Hollow Cathode Lamp and Flame.

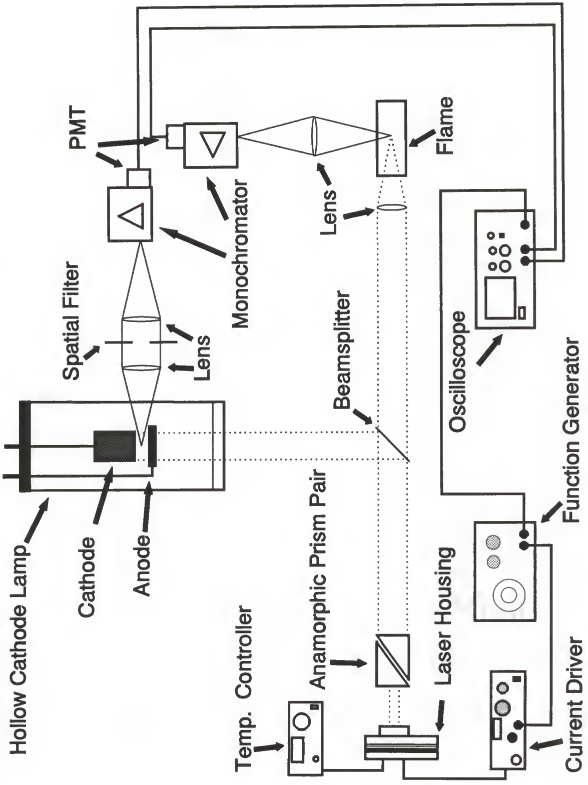
Hollow Cathode Lamp
Cathode
Anode
Temp. Controller
Anamorphic Prism Pair
Laser Housing
Current Driver
Spatial Filter
Lens
Beamsplitter
Function Generator
Monochromator
Lens
Oscilloscope
PMT
Flame

HCL and the flame. The fluorescence was focussed onto the slits of two monochromators whose slit widths were adjusted to give a 1 nm bandpass. The purpose of the monochromator was to be a narrow bandpass filter. The resolution of the spectra obtained was determined by the laser. In the case of the HCL, it was necessary to use spatial filters to reduce the laser scatter from the anode and cathode.

Results and Discussion

The absorption spectrum of the HCL is shown in Figure A-3. The hyperfine components are partially resolved (55). A Fabry-Perot interferometer was not available to calibrate the frequency of the laser emission, so it was difficult to make an assignment of the frequency of the hyperfine components. From published data, the two outer peaks are due to the ^{87}Rb isotope and the inner peaks are due to the ^{85}Rb isotope. This spectrum shows the possibility of using diode lasers for isotopic analysis.

The fluorescence spectra are shown in Figure A-4. Since the spectra were taken simultaneously, the relative shift of the peak maximum can be observed. The wavelength shifting was due to collisional broadening. It can also be seen that the assumption that the HCL is a line source is not valid for the 780.023 nm transition of rubidium.

The effect of hyperfine structure, line shift, and broadening of the HCL emission has been shown to decrease the sensitivity and cause non-linearity in

Figure A-3. Rubidium Absorption Measured in a Hollow Cathode Lamp. The x-axis is Based on Hyperfine Splitting Reported in Reference 55.

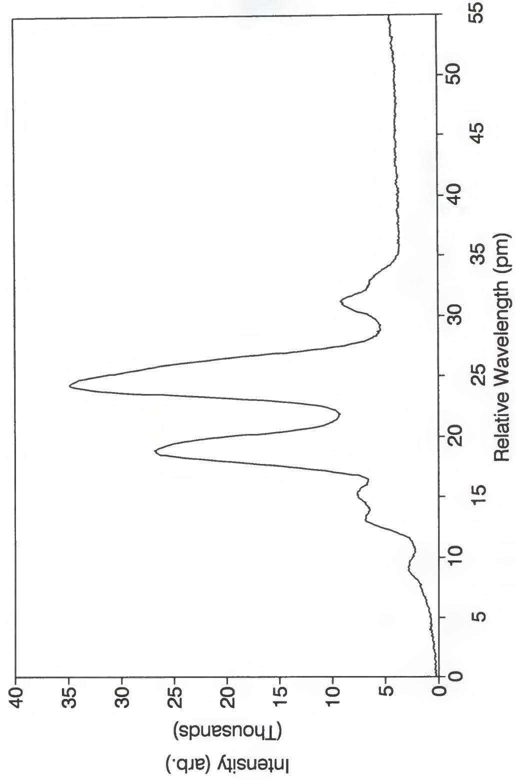
Intensity (arb.)
(Thousands)
0
5
10
15
20
25
30
35
40
Relative Wavelength (pm)
0
5
10
15
20
25
30
35
40
45
50
55

Figure A-4. Rubidium Fluorescence Measured in a Hollow Cathode Lamp and in a Flame.

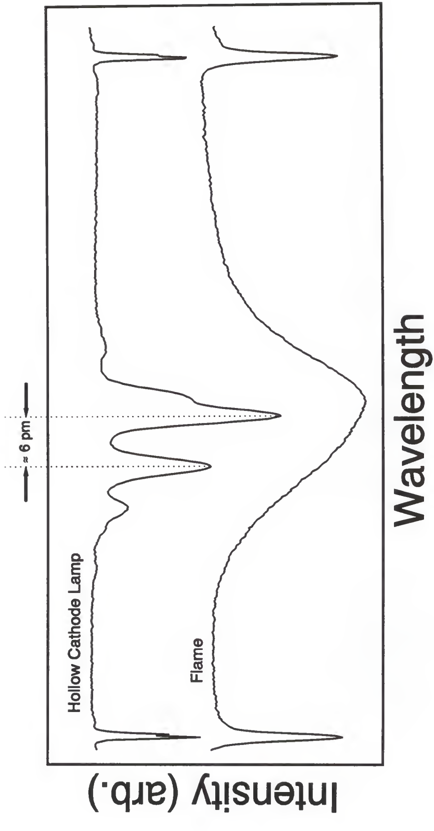
Intensity (arb.)
Wavelength
Hollow Cathode Lamp
Flame
≈ 6 pm

calibration curves. A diode laser should thus be a better source for atomic absorption. It is relatively monochromatic and can be tuned to the peak absorption for higher sensitivity. Unfortunately, as was discussed in Chapter 4, there are several difficulties associated with using a diode laser for atomic spectroscopy.

REFERENCES

1. J.D. Ingle, Jr., S.R. Crouch, Spectrochemical Analysis, Prentice Hall, Englewood Cliffs, New Jersey (1988).

2. B.W. Smith, M.R. Glick, K.N. Spears, J.D. Winefordner, Appl. Spectrosc., 43, 376 (1980).

3. 1991 Laser Focus World Buyers' Guide, Pennwell Publishing Company, Tulsa, Oklahoma (1991).

4. J. Hecht, Understanding Lasers, Howard W. Sams & Company, Ft. Worth, TX (1988).

5. D.F. Welch, Diode Lasers, Short Course Notes, Spectra Diode Labs, San Jose, California (1989).

6. Optics Guide 5, Melles Griot Corporation, Irvine, California (1991).

7. D.A. Bell, Electronic Devices and Circuits, 2nd Edition, Reston Publishing Company, Inc., Reston, VA (1980).

8. F. Su, Laser Diodes: From Electrons to Light, OE Reports, January, SPIE, Bellingham, Washington (1989).

9. G.P. Agrawal, N.K. Dutta, Long-Wavelength Semiconductor Lasers, Van Nostrand Reinhold Company, New York, (1986).

10. D. Botez, IEEE Spectrum., June, 43 (1985).

11. T. Hertsens, ILX Lightwave Application Notes, No. 5 (1989).

12. J. Lawrenz, K. Niemax, Spectrochim. Acta, 44B, 155 (1989).

13. J.C. Camparo, Contemp. Phys., 26, 443 (1985).

14. P.W. Milonni, J.H. Eberly, Lasers, John Wiley & Sons, New York (1988).

15. K. Petermann, Laser Diode Modulation and Noise, Kluwer Academic Publishers, Boston (1988).

16. C.E. Wieman, L. Hollberg, Rev. Sci. Instrum., 62, 1 (1991).

17. F. Wittgrefe, M.D. Hoogerland, J.P. Woerdman, Meas. Sci. Technol., 2, 302 (1991).

18. L. Goldberg, H.F. Taylor, A. Dandridge, J.F. Weller, R.O. Miles, IEEE J. Quant. Electron., QE-18, 555 (1982).

19. B. Bowen, D. Stanisich, ILX Lightwave Application No. 3 (1988).

20. A.P. Thorne, Spectrophysics, 2nd Edition, Chapman and Hall, New York (1988).

21. C.Th.J. Alkemade, Tj. Hollander, W. Snelleman, P.J.Th. Zeegers, Metal Vapours in Flames, Pergamon Press, New York (1982).

22. G.F. Kirkbright, M. Sargent, Atomic Absorption and Fluorescence Spectroscopy, Academic Press, New York (1974).

23. B.V. L'vov, Atomic Absorption Spectrochemical Analysis, Adam Hilger, London, UK (1970).

24. A.C.G. Mitchell, M.W. Zemansky, Resonance Radiation and Excited Atoms, The Macmillan Company, New York (1934).

25. R. Mavrodineanu, H. Boiteux, Flame Spectroscopy, John Wiley & Sons, Inc., New York (1965).

26. G. Herzberg, Atomic Spectra and Atomic Structure, 2nd Edition, Dover Publications, Inc., New York (1944).

27. M.J. Rutledge, Laser Excited Fluorescence and Ionization for Flame Diagnostics, Dissertation, University of Florida (1987).

28. B.H. Armstrong, J. Quant. Spectrosc. Radiat. Transfer, 7, 61 (1967).

29. T. Imasaka, N. Ishibashi, Anal. Chem., 62, 363A (1990).

30. B. Dahmani, L. Hollberg, R. Dullinger, Opt. Lett., 12, 876, (1987).

31. Y.C. Chung, T.M. Shay, Opt. Eng., 27, 424 (1988).

32. H. Hori, Y. Kitayama, M. Kitano, T. Yabuzaki, T. Ogawa, IEEE J. Quant. Electr., QE-19, 169 (1983).

33. J.C. Camparo, C.M. Klimcak, Am. J. Phys., 51, 815 (1983).

34. J. Lawrenz, A. Obrebski, K. Niemax, Anal. Chem., 59 770 (1236).

35. J. Lawrenz, A. Obreski, K. Niemax, Anal. Chem., 59, 1236 (1987).

36. K.C. Ng, A.H. Ali, T.E. Barber, J.D. Winefordner, Anal. Chem., 62, 1893 (1990).

37. K.C. Ng, A.H. Ali, T.E. Barber, J.D. Winefordner. Appl. Spectrosc., 44, 849 (1990).

38. K.C. Ng, A.H. Ali, T.E. Barber, J.D. Winefordner, Appl. Spectrosc., 44, 1094 (1990).

39. R. Hergenröder, K. Niemax, Spectrochim. Acta, 34B, 1443 (1988).

40. W. Demtröder, Laser Spectroscopy, Springer-Verlag, New York (1988).

41. T.E. Barber, P.E. Walters, M.W. Wensing, J.D. Winefordner, Spectrochim. Acta, 46B, 1009 (1991).

42. P.E. Walters, T.E. Barber, M.W. Wensing, J.D. Winefordner, Spectrochim. Acta, 46B, 1015 (1991).

43. P. Johnson, Semiconductor Diode Laser as an Excitation Source for Molecular and Atomic Fluorescence, Dissertation, University of Florida (1989).

44. B. Magyar, CRC Crit. Rev. Anal. Chem., 17, 145 (1988).

45. W. Slavin, G.R. Carnrick, Spectrochim. Acta, 39B, 271 (1984).

46. B.V. L'vov, Spectrochim. Acta, 33B, 153 (1978).

47. B. Magyar, K. Ikrényi, E. Bertulun, Spectrochim. Acta, 45B, 1139 (1990).

48. C.Th.J. Alkemade, Analytical Applications of Lasers, Chapter 4, E.H. Piepmeier, Ed., Wiley-Interscience, New York (1986).

49. M.J. Rutledge, B.W. Smith, J.D. Winefordner, Anal. Chem., 59, 1794 (1987).

50. B.W. Smith, M.J. Rutledge, J.D. Winefordner, Appl. Spectrosc., 41, 613 (1987).

51. T.E. Barber, P.E. Walters, J.D. Winefordner, N. Omenetto, Appl. Spectrosc., 45, 524 (1991).

52. A.M. Van der Spek, J.J.L. Mulders, C.W.G. Steenhugsen, J. Opt. Soc. Am. B., B(7), 1478 (1988).

53. A. Walsh, Spectrochim. Acta, 7, 108 (1955).

54. H.C. Wagenaar, Ph.D. Thesis, Technische Hogeschool Delft, Netherlands (1976).

55. H.M. Gibbs, R.J. Hull, Phys. Rev., 153(1), 132 (1962).

BIOGRAPHICAL SKETCH

Tye Ed Barber was born on the 24th of January, 1965 in Tampa, Florida. He graduated from the University of South Florida with a B.A. in chemistry in 1987. He received his Ph.D. in Analytical Chemistry under the direction of James D. Winefordner at the University of Florida.

I certify that I have read this study and that in my opinion it conforms to acceptable standards of scholarly presentation and is fully adequate, in scope and quality, as a dissertation for the degree of Doctor of Philosophy.

James D Winefordner

James D. Winefordner, Chairman
Graduate Research Professor of
Chemistry

I certify that I have read this study and that in my opinion it conforms to acceptable standards of scholarly presentation and is fully adequate, in scope and quality, as a dissertation for the degree of Doctor of Philosophy.

G. M. Schmid

Dr. Gerhard M. Schmid
Associate Professor of Chemistry

I certify that I have read this study and that in my opinion it conforms to acceptable standards of scholarly presentation and is fully adequate, in scope and quality, as a dissertation for the degree of Doctor of Philosophy.

Vaneica Y. Young

Vaneica Y. Young
Associate Professor of Chemistry

I certify that I have read this study and that in my opinion it conforms to acceptable standards of scholarly presentation and is fully adequate, in scope and quality, as a dissertation for the degree of Doctor of Philosophy.

Richard A Yost

Richard A. Yost
Professor of Chemistry

I certify that I have read this study and that in my opinion it conforms to acceptable standards of scholarly presentation and is fully adequate, in scope and quality, as a dissertation for the degree of Doctor of Philosophy.

Eric R. Allen
Professor of Environmental
Engineering Sciences

This dissertation was submitted to the Graduate Faculty of the Department of Chemistry in the College of Liberal Arts and Sciences and to the Graduate School and was accepted as partial fulfillment of the requirements for the degree of Doctor of Philosophy.

May, 1992

Dean, Graduate School